LETTER Communicated by George Gerstein

Unitary Events in Multiple Single-Neuron Spiking Activity: I. Detection and Significance

Sonja Grün
gruen@mpih-frankfurt.mpg.de
Department of Neurophysiology, Max-Planck Institute for Brain Research, D-60528 Frankfurt/Main, Germany

Markus Diesmann
diesmann@chaos.gwdg.de
Department of Nonlinear Dynamics, Max-Planck Institut für Strömungsforschung, D-37073 Göttingen, Germany

Ad Aertsen
aertsen@biologie.uni-freiburg.de
Department of Neurobiology and Biophysics, Institute of Biology III, Albert-Ludwigs-University, D-79104 Freiburg, Germany

It has been proposed that cortical neurons organize dynamically into functional groups (cell assemblies) by the temporal structure of their joint spiking activity. Here, we describe a novel method to detect conspicuous patterns of coincident joint spike activity among simultaneously recorded single neurons. The statistical significance of these unitary events of coincident joint spike activity is evaluated by the joint-surprise. The method is tested and calibrated on the basis of simulated, stationary spike trains of independently firing neurons, into which coincident joint spike events were inserted under controlled conditions. The sensitivity and specificity of the method are investigated for their dependence on physiological parameters (firing rate, coincidence precision, coincidence pattern complexity) and temporal resolution of the analysis. In the companion article in this issue, we describe an extension of the method, designed to deal with nonstationary firing rates.

1 Introduction

In the classical view, firing rates play a central role in neural coding (Barlow, 1972, 1992). This approach indeed led to fundamental insights into the neuronal mechanisms of brain function (Georgopoulos, Taira, & Lukashin, 1993; Hubel & Wiesel, 1977; Newsome, Britten, & Movshon, 1989). In parallel, however, a different concept was developed, in which the temporal organization of spike discharges within functional groups of neurons—

so-called neuronal assemblies (Hebb, 1949)—contribute to neural coding (von der Malsburg, 1981; Abeles, 1982b, 1991; Gerstein, Bedenbaugh, & Aertsen, 1989; Palm, 1990; Singer, 1993). It was argued that the biophysics of synaptic integration favors coincident presynaptic events over asynchronous ones (Abeles, 1982c; Softky & Koch, 1993). Accordingly, synchronized spikes are considered a property of neuronal signals that can be detected and propagated by other neurons (Diesmann, Gewaltig, & Aertsen, 1999). In addition, these spike correlations should be dynamic, reflecting varying affiliations of the neurons, depending on stimulus and behavioral context. Thereby, synchrony of firing would be directly available to the brain as a potential neural code (Perkel & Bullock, 1968; Johannesma, Aertsen, van den Boogaard, Eggermont, & Epping, 1986).

Dynamic modulations of spike correlation at various levels of precision have in fact been observed in different cortical areas: visual (Eckhorn et al., 1988; Gray & Singer, 1989; for reviews, see (Engel, König, Schillen, & Singer, 1992; Aertsen & Arndt, 1993; Singer & Gray, 1995; Roelfsema, Engel, König, & Singer, 1996; Singer et al., 1997; Singer, 1999), auditory (Ahissar, Bergman, & Vaadia, 1992; Eggermont, 1992; DeCharms & Merzenich, 1996; Sakurai, 1996), somatosensory (Laubach, Wessberg, & Nicolelis, 2000; Nicolelis, Baccala, Lin, & Chapin, 1995; Steinmetz et al., 2000), motor (Murthy & Fetz, 1992; Sanes & Donoghue, 1993; Hatsopoulos, Ojakangas, Paninski, & Donoghue, 1998), and frontal (Aertsen et al., 1991; Abeles, Vaadia, Prut, Haalman, & Slovin, 1993; Abeles, Bergman, Margalit, & Vaadia, 1993; Vaadia et al., 1995; Prut et al., 1998). Little is known, however, about the functional role of temporal organization in such signals. First hints toward the importance of accurate spike patterns came from the work of Abeles and colleagues (Abeles, Vaadia, et al., 1993; Abeles, Bergman, et al., 1993; Prut et al., 1998). They observed that multiple single-neuron recordings from the frontal cortex of awake, behaving monkeys contain an abundance of recurring precise spike patterns. These patterns had a duration of up to several hundred milliseconds, repeated with a precision of ± 1 ms, and occurred in systematic relation to sensory stimuli and behavioral events.

To test the hypothesis that cortical neurons coordinate their spiking activity into volleys of precise synchrony, we developed a method to detect the presence of conspicuous spike coincidences in simultaneously recorded multiple single-unit spike trains and to evaluate their statistical significance. We refer to such conspicuous coincidences as *unitary events* and define them as those joint spike constellations that recur more often than expected by chance (Grün, Aertsen, Abeles, Gerstein, & Palm, 1994; Grün, 1996). Briefly, the algorithm works as follows: The simultaneous observation of spiking events from N neurons is described mathematically by the joint process composed of N parallel point processes. By appropriate binning, this is transformed into an N-fold $(0, 1)$-process, the statistics of which are described by the set of activity vectors reflecting the various $(0, 1)$-constellations occurring across the neurons. Under the null hypothesis of independent firing,

the expected number of occurrences of any activity vector and its probability distribution can be calculated analytically on the basis of the single-neuron firing rates. The degree of deviation from independence is derived by comparing these theoretically derived values with their empirical counterparts. Those activity vectors that violate the null-hypothesis of independence define potentially interesting occurrences of joint-events; their composition defines the set of neurons that are momentarily engaged in synchronous activity.

To test the significance of such unitary coincident events, we developed a new statistical measure: the *joint-surprise*. For any particular activity vector, the joint-surprise measures the cumulative probability of finding the observed number of coincidences or an even larger one by chance. To account for nonstationarities in the discharge rates, modulations in spike rates and coincidence rates are determined on the basis of short data segments by sliding a fixed time window (typically 100 ms wide) along the data in steps of the coincidence bin width. This segmentation is applied to each trial, and the data of corresponding segments in all trials are analyzed as one quasi-stationary data set, using the appropriate rate approximation.

Having first ascertained the statistical significance of brief epochs of synchronous spiking, the functional significance of such unitary coincident events is then tested by investigating the times of their occurrence and their composition in relation to sensory stimuli and behavioral events. Thus, Riehle, Grün, Diesmann, and Aertsen (1997) found that simultaneously recorded activities of neurons in monkey primary motor cortex exhibited context-dependent, rapid changes in the patterns of coincident action potentials during performance of a delayed-pointing task. Accurate spike synchronization occurred in relation to external events (visual stimuli, hand movements), commonly accompanied by discharge rate modulations, however, without precise time locking of the spikes to these external events. Accurate spike synchronization also occurred in relation to purely internal events (stimulus expectancy), where firing-rate modulations were distinctly absent. These findings indicate that internally generated synchronization of individual spike discharges may subserve the cortical organization of cognitive motor processes. The clear correlation of the precise spike coincidences with behavioral events was interpreted as evidence for their functional relevance (Riehle et al., 1997; Fetz, 1997).

Thus, unitary event analysis evoked a considerable amount of interest in the ongoing debate on spike synchronization (Shadlen & Newsome, 1998; Diesmann et al., 1999) and its detectability in experimental data (Pauluis & Baker, 2000; Roy, Steinmetz, & Niebur, 2000; Gütig, Aertsen, & Rotter, in press). It is currently used in a number of laboratories (Pauluis, 1999; Grammont & Riehle, 1999; Riehle, Grammont, Diesmann, & Grün, 2000). Here we provide for the first time a full account of the unitary event method and discuss its underlying principles in detail. In this article, we describe

the theory and statistical background of the analysis method for stationary conditions—when the firing rates of the neurons under observation do not change as a function of time. Simulated spike trains, consisting of parallel, independent Poisson processes into which we inserted particular coincident spike constellations under controlled conditions, were used to test and calibrate the method. In the companion article in this issue, we extend the method to deal with nonstationary firing rates and to illustrate its potential by analyzing multiple single-neuron recordings from frontal and motor cortical areas in awake, behaving monkeys. Preliminary descriptions of the method have been presented in abstract form (Grün, Aertsen, Abeles, & Gerstein, 1993; Grün et al., 1994; Grün & Aertsen, 1998) and in Riehle et al., (1997).

2 Detecting Unitary Events in Joint Spiking Activity

2.1 Representation of Joint Spiking Activity. By introducing a temporal resolution Δ, the spike train of a single neuron i recorded over a time interval of length $\mathcal{T}$ can be represented by a binary process $v_i(t)$, that is, as a (0, 1)-sequence. With $T = \lfloor \mathcal{T}/\Delta \rfloor$ denoting the total number of time steps, we define

$$v_i(t) = \begin{cases} 1, & \text{if spike in } [t, t+\Delta) \\ 0, & \text{if no spike in } [t, t+\Delta), \end{cases}$$
$$t = 0, 1\Delta, 2\Delta, \ldots, (T-1)\Delta. \tag{2.1}$$

The minimal Δ is set by the spike time resolution h (in the data we analyzed, typically 1 ms). In our analysis, we used integer multiples of the data resolution $\Delta = bh$ for the binning grid, with b serving as a control parameter for the analysis precision (Δ is called analysis *bin size*). Thus, each point in time is assigned to a unique bin, which we refer to as *exclusive binning*. A single bin, however, may contain more than one spike. Equation 2.1 guarantees that $v_i(t)$ is restricted to 1, even if the corresponding bin contains more than one spike, which we refer to as *clipping*.

The simultaneous observation of spike events from N neurons can now be represented in this binary framework. The activities of the individual neurons i are described by parallel binary sequences $v_i(t)$. Alternatively, we can describe the N sequences as a single sequence of a vector-valued function $\mathbf{v}(t)$, the components of which are formed by the $v_i(t)$:

$$\mathbf{v}(t) = \begin{bmatrix} v_1(t) \\ \vdots \\ v_i(t) \\ \vdots \\ v_N(t) \end{bmatrix}, \quad i = 1, \ldots, N; \; v_i \in \{0, 1\}. \tag{2.2}$$

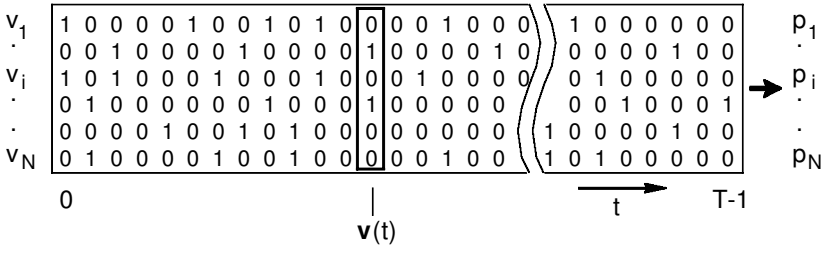

Figure 1: N parallel binary processes, lasting for T time steps. Each horizontal row, consisting of a sequence of 0s and 1s, represents a realization of a single process v_i. The 1s mark the occurrences of spike events. The joint activity across the processes at each instant in time can be expressed by a vector $\mathbf{v}(t)$, as indicated for one example. The empirical firing probability per bin p_i of each single process is evaluated as the marginal probability: the number of spikes in the observation time interval, divided by the number of time steps.

This scheme is illustrated in Figure 1. At each time step, $\mathbf{v}(t)$ equals one of the $m = 2^N$ possible constellations of 0s and 1s (*coincidence patterns*). The m possible constellations $\mathbf{v}^k$ are identified by a (for now) arbitrary index function k (e.g., let $\mathbf{v}^k$ be mapped to an integer $k \in \{1, \ldots, m\}$ by interpreting $\mathbf{v}^k$ as the binary representation of an integer $(v_N^k \ldots v_1^k)_2$ and defining $k = (v_N^k \ldots v_1^k)_2 + 1$). The empirical number of occurrences of a coincidence pattern $\mathbf{v}^k$ in data recorded over an interval T is called n_k.

2.2 The Null-Hypothesis of Independent Firing. We are interested in detecting the (sub)groups of neurons jointly involved in a cell assembly—the neurons that act in an interdependent manner. To distinguish these neurons from those that are not involved, we develop a statistical tool to test the null hypothesis (H_0) of independent neurons.

Under this null-hypothesis, the joint-probability $P_k = P(\mathbf{v}^k)$ of a coincidence pattern $\mathbf{v}^k$ (a particular constellation of spikes and nonspikes across the observed neurons) equals the product of the probabilities of the individual events:

$$H_0\colon\ P_k = \prod_{i=1}^{N} P\left(v_i^k\right),$$
$$\text{with } P\left(v_i^k\right) = \begin{cases} P\left(v_i = 1\right), & \text{if } v_i^k = 1 \\ 1 - P\left(v_i = 1\right), & \text{if } v_i^k = 0. \end{cases} \tag{2.3}$$

Equation 2.3 assumes independence of the N neuronal processes. In addition, we now make the assumption that the binary sequence describing the activity of a single neuron (equation 2.1) represents a sequence of Bernoulli

trials (Feller, 1968). The probability of a specific outcome $v_i(t)$ does not depend on the value of v_i at any other point in time. A Poisson process, often used to model neuronal spike trains (see section 5), leads to a binary sequence in accordance with the above assumption. Equation 2.3 is based on precise knowledge of the single-neuron firing probabilities $p_i = P(v_i = 1)$. However, in the experimental situation, the firing probabilities are typically unknown and have to be estimated from the data. The simplest scheme is to adopt the frequency interpretation (e.g., Feller, 1968) and use the number of spike events c_i in the observation interval $\mathcal{T}$ containing T time steps to calculate the probability $p_i = c_i/T$ as an estimate for the firing probability of neuron i (for an alternative approach, see Gütig et al., in press).

The task now is to develop a tool that enables us to judge whether the empirical number of occurrences n_k^{emp} of a particular coincidence pattern $\mathbf{v}^k$ deviates significantly from the expected number n_k^{pred}.

2.3 Describing Independently Spiking Neurons by Multiple Bernoulli Trials. Consider a set of parallel realizations of the N binary processes with duration T. The N resulting T-dimensional row vectors can be combined to a matrix of 0s and 1s with N rows and T columns (see Figure 1). According to the assumptions made in the previous section, the probability of a particular outcome in a specific matrix element does not depend on the outcome in any of the other matrix elements. Equivalently, we can describe the realization as a succession of T N-dimensional column vectors (coincidence patterns). A process generating such N-dimensional events is called a multiple Bernoulli trial (Feller, 1968). Following Feller (1968), we can write the probability of finding each pattern $\mathbf{v}^k$ exactly n_k times in the observation interval directly in terms of the P_k:

$$\psi(n_1, n_2, \ldots, n_m; P_1, P_2, \ldots, P_m; T) = \frac{T!}{\prod_{k=1}^{m} n_k!} \cdot \prod_{k=1}^{m} P_k^{n_k}. \tag{2.4}$$

This expression represents a generalization of the binomial distribution to a process with more than two possible outcomes and is called a multinomial distribution. The P_k and n_k are subject to the normalizing conditions

$$\sum_{k=1}^{m} P_k = 1 \tag{2.5}$$

$$\sum_{k=1}^{m} n_k = T. \tag{2.6}$$

For any particular spike constellation $\mathbf{v}^k$ (defining that particular $\mathbf{v}^k$ as "the" outcome and all the rest as "the others"), the probability distribution in equation 2.4 can be reduced to the binomial distribution. For such selected

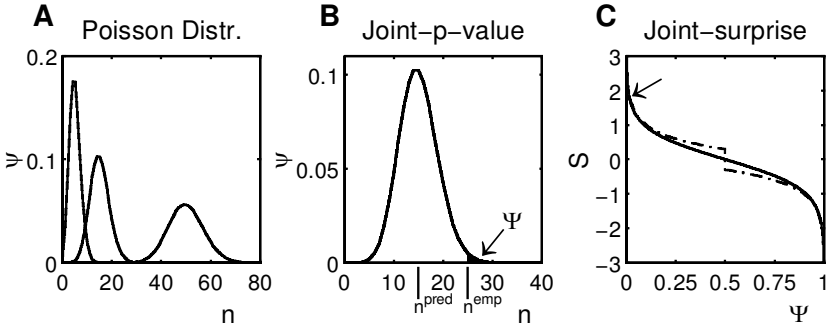

Figure 2: (A) Three examples of Poisson distributions, for parameters $n^{\text{pred}} = 5, 15$, and 50 (from left to right). (B) The black shaded area under the Poisson distribution ($n^{\text{pred}} = 15$), ranging from $n^{\text{emp}} = 25$ to infinity, indicates the joint-p-value Ψ as the cumulative probability. For this example, the joint-p-value equals 0.0112. (C) The joint-surprise S shown as a logarithmic scaling function of the joint-p-value. The dash-dotted line equals the surprise measure as defined by Palm (1981), and the solid line shows the continuous, differentiable version used here: the joint-surprise (see equation 2.10). The value of the joint-surprise corresponding to the joint-p-value in the example in B is 1.9459.

constellation $\mathbf{v}^k$, we obtain

$$\psi(n_k; P_k; T) = \frac{T!}{n_k! \cdot (T - n_k)!} \cdot P_k^{n_k} \cdot (1 - P_k)^{T - n_k}, \quad k = 1, \ldots, m. \tag{2.7}$$

Since the number of time steps T (or $T_b = T/b$ for a binning grid b) is usually large for bh in the order of 1 ms and the associated probabilities P_k are small, while their product $P_k \cdot T$ remains moderate, equation 2.7 can be approximated by the Poisson distribution (Feller, 1968; see Figure 2A):

$$\psi\left(n_k; P_k; T\right) = \frac{(P_k \cdot T)^{n_k}}{n_k!} \cdot \exp\left(-P_k \cdot T\right), \quad k = 1, \ldots, m. \tag{2.8}$$

Here, $P_k \cdot T$ is the rate parameter of the Poisson distribution, defining the expected number of occurrences $n_k^{\text{pred}} = P_k \cdot T$ of the joint spike constellation $\mathbf{v}^k$.

2.4 Significance of Joint-Events: The Joint-Surprise. For each of the m constellations $\mathbf{v}^k$ in the observation set, equation 2.7 describes the null-hypothesis of independent component processes. The expected number of occurrences $n_k^{\text{pred}} = P_k \cdot T$ defines the center of mass of the distribution.

Thus, for each empirical number of occurrences n_k^{emp}, we can now compute the statistical significance of the deviation from independence. It is defined as the cumulative probability of finding the observed number of occurrences n_k^{emp} or an even larger one (an alternative approach of measuring deviation from independence using the framework of information theory is discussed in appendix C). We call this cumulative probability the *joint-p-value* Ψ, defined by

$$\begin{aligned}
&\Psi\left(n_k^{\text{emp}} \mid n_k^{\text{pred}}\right) \\
&\quad = \sum_{n_k=n_k^{\text{emp}}}^{\infty} \psi\left(n_k, n_k^{\text{pred}}\right) \\
&\quad = \sum_{n_k=n_k^{\text{emp}}}^{\infty} \frac{\left(n_k^{\text{pred}}\right)^{n_k}}{n_k!} \cdot \exp\left(-n_k^{\text{pred}}\right), \qquad k = 1, \ldots, m. \qquad (2.9)
\end{aligned}$$

It can efficiently be evaluated numerically using the connection to the regularized incomplete gamma function (Press, Teukolsky, Vetterling, & Flannery, 1992). Figure 2B shows Ψ as the black area under the distribution. The smaller this area is, the higher is the significance of the corresponding count:

$$\begin{array}{llll}
\text{if} & n_k^{\text{emp}} > n_k^{\text{pred}} & \text{then} & 0 \leq \Psi < 0.5 \\
\text{if} & n_k^{\text{emp}} \simeq n_k^{\text{pred}} & \text{then} & \Psi \simeq 0.5 \\
\text{if} & n_k^{\text{emp}} < n_k^{\text{pred}} & \text{then} & 0.5 < \Psi \leq 1.
\end{array}$$

Thus, the larger the number of excessive coincidences, the closer Ψ is to 0.

By similar reasoning, we can define the statistical significance for coincidence patterns occurring at an unexpectedly low rate (i.e., "lacking" coincidences). The statistical significance of finding at most n_k^{emp} repetitions of pattern $\mathbf{v}^k$ is obtained as the complementary part of the sum in equation 2.9 ($n_k = 0, \ldots, n_k^{\text{emp}}$). In that case, the lower the number of coincidences is (or, the larger the number of lacking ones), the closer Ψ is to 1 and the closer its complement $1 - \Psi$ is to 0.

To enhance the visual resolution at the relevant low values for Ψ (or $1-\Psi$), one may choose a logarithmic scaling as was done for the surprise measure (Legendy, 1975; Palm, 1981; Legendy & Salcman, 1985; Palm, Aertsen, & Gerstein, 1988; Aertsen, Gerstein, Habib, & Palm, 1989). This is a straightforward scale transformation, defined as $-\log(\Psi)$ for Ψ larger than 0.5 and as $-\log(1-\Psi)$ for Ψ smaller than 0.5. However, since this function is discontinuous at $\Psi = 0.5$ (see Figure 2C, dotted line) it leads to wildly fluctuating values when considering Ψ-values close to chance level. To overcome this problem, we define a new transformation, the joint-surprise, which approx-

imates the conventional surprise measure for the relevant values of Ψ and yields a continuous and differentiable function around $\Psi = 0.5$:

$$S(\Psi) = \log \frac{1 - \Psi}{\Psi}. \tag{2.10}$$

For excessive coincidences, this function is dominated by the numerator Ψ; for lacking coincidences, it is dominated by the denominator $1 - \Psi$ (see Figure 2C, solid line). It turns out that the expression for the joint-surprise (equation 2.10) is equivalent (apart from minor details) to the difference of the surprise for excitation and surprise for inhibition used in Palm et al. (1988) and Aertsen et al. (1989). Equation 2.10 is comparable to measure significance on a dB scale and yields positive numbers for excessive coincidences (e.g., $S = 1$ for $\Psi = 0.1$, or $S = 2$ for $\Psi = 0.01$), negative numbers for lacking ones, while changing sign at chance level $\Psi = 0.5$:

$$\begin{aligned} &\text{if} \quad n_k^{\text{emp}} > n_k^{\text{pred}} \quad &&\text{then} \quad S > 0 \\ &\text{if} \quad n_k^{\text{emp}} \simeq n_k^{\text{pred}} \quad &&\text{then} \quad S \simeq 0 \\ &\text{if} \quad n_k^{\text{emp}} < n_k^{\text{pred}} \quad &&\text{then} \quad S < 0. \end{aligned}$$

2.5 Unitary Events: Definition and Detection. On the basis of the joint-surprise as a measure of significance, we now define unitary events as those joint spike events $\mathbf{v}^k$ in a given interval $\mathcal{T}$ that occur much more often than expected by chance. To that end, we set a threshold S_α on the joint-surprise measure and denote the occurrences of those $\mathbf{v}^k$ for which

$$S\left(n_k^{\text{emp}} \mid n_k^{\text{pred}}\right) \geq S_\alpha \tag{2.11}$$

as unitary events. The arguments of $S(n_k^{\text{emp}} \mid n_k^{\text{pred}})$ remind us that this test is performed separately for each coincidence pattern $\mathbf{v}^k$ in the interval $\mathcal{T}$.

The raster display (or dot display) is the standard tool used by the electrophysiologist to look for temporal structure in the "raw" spike data (see Figure 3). Since we are interested in the dynamics of assembly activation, we want to detect the joint spike constellations that possibly express assembly activity as they occur in time. To visualize occurrences of potentially interesting coincidence patterns in relation to other instances of itself, other patterns, or other events (e.g., behavioral, stimuli), we mark all spikes in all instantiations of a significant pattern $\mathbf{v}^k$ by squares (see Figure 3, lower row). For any S_α, there is necessarily a certain probability of detecting a $\mathbf{v}^k$ as significant in a realization of independent processes (false positive). Given a realization of dependent processes generating a surplus of $\mathbf{v}^k$, there is a certain probability not to detect the pattern as significant (false negative). To obtain maximum sensitivity while maintaining a minimum level of false

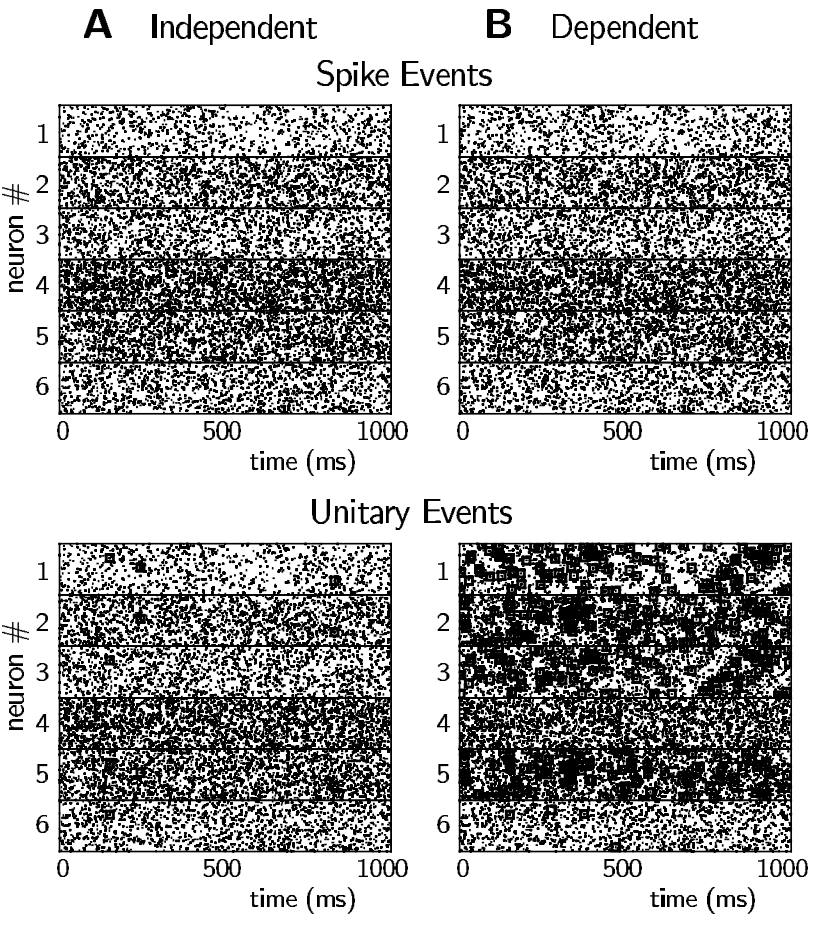

Figure 3: Dot displays in the two top panels show the simultaneous activity of six simulated neurons: independent (A) and dependent (B) firing. Firing rates are: neuron 1: 10 s^{-1}; 2: 20 s^{-1}; 3: 15 s^{-1}; 4: 30 s^{-1}; 5: 25 s^{-1}; 6: 15 s^{-1}. The spike trains in *B* are generated by first copying the spike trains of *A*. Dependencies between neurons are then introduced by injecting coincident events, consisting of neuron pairs 1,3 and 2,5 (both at coincidence rate of 1 s^{-1}), randomly distributed in time over all the trials. Each box contains the spike activity of a single neuron over 100 trials of 1000 ms duration. Each dot represents a spike at the time of its occurrence. Trials are organized in rows. Bottom panels: Spikes belonging to statistically significant constellations (unitary events) are marked by squares. Observe the different numbers of occurrences of unitary events in *A* and *B* due to the injected coincidences. In addition, in *B*, some of the constellations containing the injected spikes as subpatterns are also detected as significant events.

positives (see elaboration in section 4), we set the threshold S_α to a level between 1.28 and 2. This corresponds to a significance level α between 0.05 and 0.01, a commonly used threshold level in statistical significance tests (e.g., Hays, 1994, "p-value").

The coincidence patterns $\mathbf{v}^k$ contain different numbers of spikes ranging from 0 to N. We call the number of spikes in a pattern *complexity*:

$$\xi(\mathbf{v}^k) = \sum_{i=1}^{N} v_i^k. \tag{2.12}$$

There are $\binom{N}{\xi}$ patterns of complexity ξ. Because each of the patterns is assigned a complexity $\xi \in \{0, \ldots, N\}$, we recover the total number of patterns by the binomial theorem,

$$\sum_{\xi=0}^{N} \binom{N}{\xi} = 2^N.$$

The single pattern of complexity 0 (no spike) and the N patterns of complexity 1 (spike from one neuron) do not represent joint spiking activity in the natural sense. Therefore, we typically concentrate on patterns with $\xi(\mathbf{v}^k) > 1$. For a significant $\mathbf{v}^k$ with $\xi > 1$, each square in a dot display has a counterpart in at least one other box of the dot display at the same time instant.

The procedure is illustrated in Figure 3A for simulated realizations of six independent processes and in Figure 3B for six dependent parallel processes. Here, all patterns with $\xi(\mathbf{v}^k) > 1$ are tested independently using equation 2.11, and all significant occurrences are marked according to the convention. However, there is no need to visualize all patterns simultaneously. In an application of the method to experimental data, it might be useful to generate separate raster displays for individual patterns or subsets of patterns.

The simulation, like all further simulations, was performed as follows. Several (here $N = 6$) spike trains of 100s duration were generated using independent homogeneous Poisson processes, each with a particular rate parameter λ_i. The single spike trains were then combined, as if they had been recorded simultaneously from as many neurons. For visualization, spike data are organized in 100 consecutive trials of 1s duration (see Figure 3). Time resolution was set to $h = 1$ ms. In addition, into one of the data sets (see Figure 3B) we introduced statistical dependencies by injecting pairs of simultaneous spikes into the spike trains of neuron pairs 1, 3 and 2, 5, respectively. Both coincidences occurred at a rate of $1\ \mathrm{s}^{-1}$ and were randomly distributed in time, such that on average, each trial contained one injected coincident event. In the context of this article, it is important to note that spike trains were generated by stationary processes and that the analysis was performed once, taking into account the entire data set. "Trials"

are introduced here only for visualization. An equivalent description is that each box in Figure 3 displays the activity of a neuron as a page of text (i.e., written left to right and top to bottom). The concept of a trial becomes important only when treating nonstationary data (see the companion article). When data are organized in trials, T is understood to specify the duration of a trial (in time steps) and $M \cdot T$ is the duration of the full data set, with M indicating the number of trials.

As expected, the raster displays of the two data sets look very similar (Figure 3, top row). Since the rate of injected coincident spikes ($1\ s^{-1}$) is low compared to the baseline firing rates, comparison of corresponding firing rates in the two data sets does not reveal any noticeable difference (not shown here). The analysis for unitary events was performed with the threshold level set at $\alpha = 0.05$. With $2^N - \binom{N}{1} - \binom{N}{0} = 57$ patterns independently tested at $\alpha = 0.05$, we expect to find 2.85 patterns to be marked as significant. Observe that the dependent data set in Figure 3B (bottom) exhibits many unitary events, whereas the independent data in Figure 3A (bottom) set has almost none. Moreover, the few unitary events in the independent data set consist of spike patterns of complexity 3 and 4, appearing three and one times, respectively. Their significance is due to statistical fluctuations (we will return to this dependence on pattern complexity). In the dependent data set, however, almost all significant constellations correspond to the injected coincidences (between neurons 1 and 3, and neurons 2 and 5). In addition, some higher-order constellations containing the injected spikes as subpatterns also appear as unitary events, leading to the few squares in the raster display of neuron 6. As was to be expected from the random insertion times of the injected coincidences, the unitary events appear randomly distributed over time and trials. In real neuronal data, however, their times of occurrence may provide information concerning the dynamics of these potentially interesting constellations and their relation to stimuli or behavioral events (Riehle et al., 1997).

3 Dependence of Joint-Surprise on Physiological Parameters

Having derived the joint-surprise as a measure for statistical significance of joint spiking events, we now investigate its performance with respect to various physiologically relevant parameters: the firing rates of the neurons under consideration, the time resolution (bin size) chosen for the analysis, the rate of spike coincidences, their coincidence accuracy (allowing the biological system some degree of noise), and the number of neurons involved. To this end, we calibrate the performance of the joint-surprise by applying it to appropriately designed sets of simulated data. As before, the control data sets consist of independently generated Poisson trains of varying base rates. These are compared to different data sets, containing additionally injected coincidences of varying complexities and coincidence rates. Typically, the

simulated data consisted of $M = 100$ trials of 1000 ms each and a time resolution of $h = 1$ ms. The rates of the random Poisson trains were chosen to cover a physiologically realistic range for cortical neurons—between 10 and 100 s^{-1}.

3.1 Influence of the Firing Rate. To investigate the influence of the neurons' firing rates, we studied two parallel spike trains generated as independent Poisson processes, with both the same and constant rate. We varied this rate from $\lambda = 10$ to 100 s^{-1} in steps of 10 s^{-1}, in the presence of different constant injection rates λ_c. Expectation values for the number of coincidences in the data set n^{emp} and the number of coincidences expected to occur assuming independence n^{pred} are:

$$\begin{aligned} n^{\text{emp}} &= \left[\lambda_c h + (\lambda h)^2\right] \cdot MT \\ n^{\text{pred}} &= [(\lambda_c + \lambda)h]^2 \cdot MT. \end{aligned} \tag{3.1}$$

The probability per time step for a coincidence in the presence of injected coincidences is the sum of the probability of seeing an injected coincidence $\lambda_c h$ and seeing a chance coincidence $(\lambda h)^2$. For experimental data, we have to estimate the firing rates from the data set. The marginal probabilities (spike count divided by time interval) cannot distinguish between the base rate and the injection rate. Therefore, we obtain $\lambda_c + \lambda$ as the expectation value for the firing rate and $[(\lambda_c + \lambda)h]^2$ as the expectation value for the probability to find a coincidence assuming independence. Further corrections for the specific injection process are discussed in Grün, Diesmann, Grammont, Riehle, and Aertsen (1999). Values obtained for n^{emp} and n^{pred} in different realizations fluctuate around their expectation values. To visualize the effect of statistical fluctuations, we generated 10 data sets for each rate level. Figure 4A (top) shows that the empirical numbers of coincidences n^{emp} (diamonds) indeed match the number expected assuming independence n^{pred} (solid lines), apart from small statistical fluctuations. The number of coincidences exhibits a convex dependence on background firing rate. From equation 3.1, we know that the increase is quadratic, $(h^2 \cdot MT)$ being the coefficient of the leading power. At $\lambda = 0$, that is, only injected spikes in both situations, the expectation values n^{emp} and n^{pred} are $(\lambda_c h) \cdot MT$ and $(\lambda_c h)^2 \cdot MT$, respectively. Comparison of the expressions for n^{emp} and n^{pred} in equation 3.1 shows that in the regime $(\lambda_c + 2\lambda)h < 1$, the difference decreases linearly with λ. Variability in counts increases with firing rate because of the well-known property of the Poisson distribution (see equation 2.8) that the count variance equals the mean. Figure 4 (top row) demonstrates that also the expected number of coincidences assuming independence n^{pred} exhibits fluctuations. These fluctuations are caused by the fact that the firing rates have to be estimated from the data. The variance is given by

$$\sigma^2_{n^{\text{pred}}} = [(\lambda + \lambda_c)h]^2 \, (2\lambda + 4\lambda_c)h \cdot MT, \tag{3.2}$$

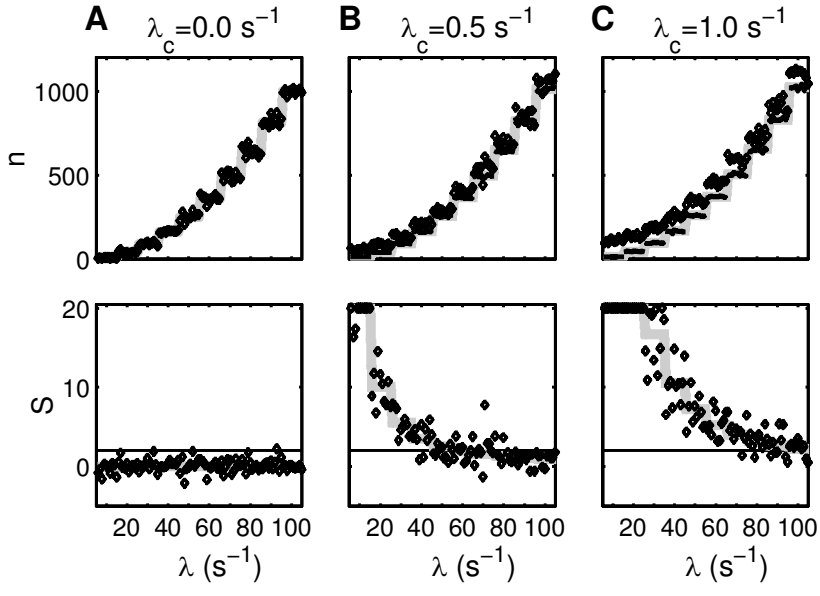

Figure 4: Detection of coincident events under different firing-rate conditions. Simulated data from two parallel processes were analyzed for the presence of coincident events. Realizations consisting of 100 trials, each of duration 1000 ms, were generated with a time resolution of 1 ms. Rates of both processes were varied from 10 to 100 s^{-1} in steps of 10 s^{-1}. The experiment was repeated 10 times at each rate, to visualize statistical variations. Coincident events, also generated by Poisson processes, were injected into each of the 10 data sets at one of two coincidence rates (B: $0.5s^{-1}$, C: $1s^{-1}$). The results of the control experiments without injected events are shown in A. Data were analyzed for the number of empirical occurrences (top row, diamonds) versus expected level (top row, solid lines, theoretical curve in gray), estimated from the marginal probabilities. The corresponding joint-surprise is shown in the bottom panels (diamonds, theoretical curve in gray). Results for the 10 realizations per firing rate are grouped together, giving rise to the stairway-like appearance of the plots. Horizontal lines in the bottom panels indicate the significance threshold ($\alpha = 0.01$).

which, with $\lambda_c < \lambda$, is bounded by

$$\lessapprox 3\,[(\lambda + \lambda_c)h]^3 \cdot MT. \tag{3.3}$$

This dependence on the third power in λh renders it much smaller than the variance of n^{emp} in the parameter range of interest (say, $\lambda h < \frac{1}{6}$, $\lambda_c < \lambda$).

Closely related to the probability of obtaining false positives (significant outcome in the absence of excess coincidences; see section 4) is the question of how precisely n^{pred} can be estimated when no coincidences are injected.

Comparing the variance of the coincidence counts when no coincidences are injected $(\lambda h)^2 \cdot MT$ with equation 3.2 for $\lambda_c = 0$ suggests that above $\lambda h = \frac{1}{2}$, the variance of n^{pred} exceeds the variance of n^{emp}. However, at this high probability, the Poisson distribution is no longer a good approximation. Using the binomial distribution (see equation 2.7) in the argument above, it turns out that the variance of n^{pred} is always smaller than the variance of n^{emp}. The insight gained by analyzing the variances of n^{pred} and n^{emp} to understand the fluctuations of S is limited, because the two measures are not completely independent: a high spike count for one of the neurons simultaneously leads to high values for n^{pred} and n^{emp}. We present an analysis of the relation of significance level α to the percentage of false positives obtained in independent data sets in section 4.

Figure 4 (bottom row) shows the joint-surprise values corresponding to the $(n^{\text{pred}}, n^{\text{emp}})$ pairs (top row). Without injected coincidences, the joint-surprise fluctuates around 0, independent of the rate, due to the fluctuations in n^{emp} and n^{pred}. Because we necessarily have fluctuations in n^{pred}, the percentage of experiments in which the coincidence count is significant may differ from the theoretical value (assuming a known n^{pred}) determined by S_α (see section 4). In the case of injected coincident events, the measured and expected coincidence counts deviate from each other, and the more so the higher the injection rate (for Figure 4B, $0.5\,\text{s}^{-1}$; for Figure 4C, $1\,\text{s}^{-1}$). The joint-surprise declines hyperbolically with increasing background rate due to the decreasing ratio $(n^{\text{emp}} - n^{\text{pred}})/n^{\text{pred}}$. At vanishing background firing rate, the expected number of coincidences assuming independence $(\lambda_c h)^2 \cdot MT$ is practically 0, while the number of measured coincidences $(\lambda_c h) \cdot MT$ remains considerable. Therefore, the joint surprise obtains a large, finite value (not shown).

For the injected coincident rate of $\lambda_c = 0.5\text{s}^{-1}$ (Figure 4B), the joint-surprise falls below the significance level of 0.01 (horizontal line in bottom graph) at a rate of about $60\ \text{s}^{-1}$ (in total, 30 trials below significance level). For the injected rate of $\lambda_c = 1.0\text{s}^{-1}$ (Figure 4C), this occurs only at a considerably higher background rate (about $100\ \text{s}^{-1}$). At higher firing rates, more excess coincident events are needed to escape from the statistically expected fluctuation range. Clearly, this behavior imposes a severe limit on the detectability of excess coincidences at high firing rates. Before the expectation of the joint-surprise falls below the significance threshold, the cloud of joint-surprise values obtained in the individual experiments has already reached it (in Figures 4B and 4C, $40\ \text{s}^{-1}$ and $70\ \text{s}^{-1}$, respectively).

However, there is a large regime where fluctuations in the joint-surprise are well separated from the significance threshold, and, hence, excess coincidences can reliably be detected. When injected coincidences are present, the difference between n^{emp} and n^{pred} increases linearly with T, while the width (standard deviation) of the joint-p-value Ψ increases with $\sqrt{T}$. Therefore, given enough data, excess coincidences can always be detected.

3.2 Influence of Binning. The time resolution of data acquisition in extracellular spike recordings is typically 1 ms or better. There is recent experimental evidence from cross-correlation, joint peristimulus time histogram (JPSTH), and, particularly, from spike pattern analysis, that the timing accuracy of spiking events that might be relevant for brain function can be as precise as 1–5 ms (Abeles, Bergman, et al., 1993; Riehle et al., 1997). Similar suggestions come from modeling studies (Diesmann et al., 1999). Here, we want to investigate whether, by choosing a binning grid $\Delta = bh$ (see equation 2.1) in that time range, we may be able to detect coincidences with corresponding accuracy. Therefore, we will first study the general influence of binning on the outcome of joint-surprise analysis and then address the effect of varying bin size on the detection of coincidences with a finite temporal jitter.

We generated a set of simulated data as before. While the rate of the independent processes was maintained constant ($20\ s^{-1}$), we injected additional coincident events at various rates. Two examples for coincident rates of $0.5\ s^{-1}$ and $1.0\ s^{-1}$ are shown in Figures 5B and 5C; the control set is shown in Figure 5A. In the analysis, we gradually increased the binning grid from $b = 1$ to $b = 10$. If there were more than one spike per bin, the result was set to one (clipping). This newly generated process formed the basis of our investigation.

Binning has two opposite effects on the coincidence counts: it reduces the number of time steps, $T_b = T/b$, while increasing the probability p_b to observe an event in a time step, compared to the original probability $p = \lambda h$. The net effect of binning is therefore comparable to that of increasing the rate while reducing the number of observation time steps. Within a single analysis bin of size bh, the probability of finding exactly k of the b possible positions occupied by a spike is given by the binomial distribution. Thus, the probability of finding one or more events $P(k \geq 1) = 1 - P(k = 0)$ equals

$$p_b = \sum_{k=1}^{b} \binom{b}{k} p^k (1-p)^{b-k} = 1 - (1 - \lambda h)^b. \tag{3.4}$$

For $p \ll 1$, it can be approximated by $p_b = b \cdot p$. Following equation 3.1, the expectation values for the number of coincidences are now

$$\begin{aligned} n_b^{\text{emp}} &= \left[\lambda_c bh + \left(1 - (1 - \lambda h)^b\right)^2\right] \cdot M \cdot T_b \\ n_b^{\text{pred}} &= \left[1 - \left(1 - (\lambda_c h + \lambda h)\right)^b\right]^2 \cdot M \cdot T_b. \end{aligned} \tag{3.5}$$

Improvements of expressions 3.5, not relevant in this context, can be made by taking into account interactions of the background spikes and the injected spikes in the binning process (Grün et al., 1999).

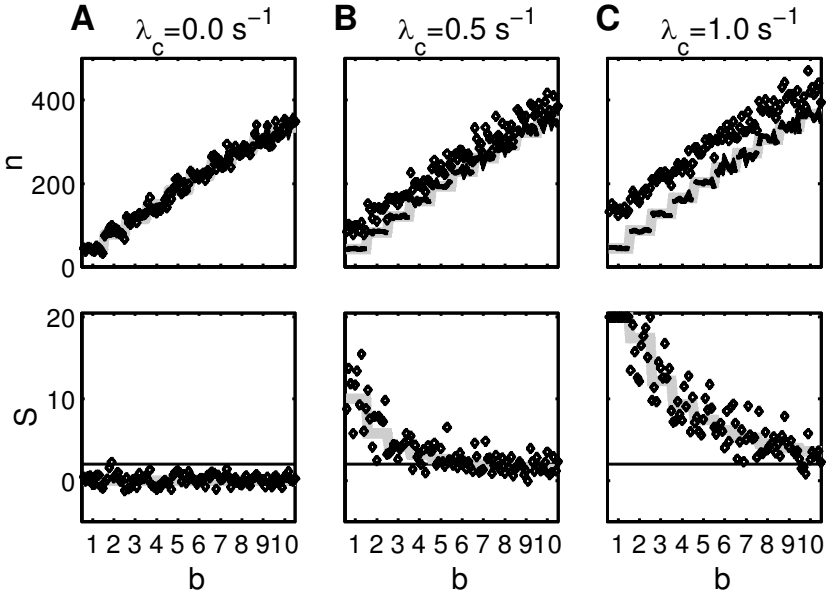

Figure 5: Detection of coincident events using different analysis bin sizes bh. Simulated data from two parallel processes were analyzed for the presence of coincident events. Realizations consisting of 100 trials, each of duration 1000 ms, were generated with a time resolution of 1 ms. Rates of both processes were kept constant at 20 s^{-1}. Coincident events were injected at different rates: (A) no injected events, (B) 0.5 s^{-1}, (C) 1.0 s^{-1}. The experiment was repeated 10 times at each bin size, to visualize statistical variations. The bin width bh was varied from 1 to 10 ms. Data were analyzed for the number of coincidences (top row, diamonds) and compared to the expected number of coincidences assuming independence (top row, solid lines, theoretical curve in gray). The corresponding joint-surprise is shown in the bottom panels (diamonds, theoretical curve in gray). Further details as in Figure 4.

n_b^{pred} is concave with positive slope for small b, reaches a maximum, and after passing a point of inflection approaches the curve T/b from below. The latter represents an upper bound for the expectation value, reached when each bin is occupied. The initial concave increase can be observed in the simulated data for n_b^{pred} as well as for n_b^{emp} (Figure 5, top row). As in the case of increasing background rate (see Figure 4), the difference between the measured and the expected coincidence counts assuming independence decreases with increasing bin size. The effect can clearly be seen at the high coincidence rate (1 s^{-1}; Figure 5C, top), less so at the lower one (0.5 s^{-1}; Figure 5B, top). In the regime shown, binning increases occupa-

tion probability (somewhat stronger for n_b^{pred} than for n_b^{emp}), and clipping is not dominant yet. In Figure 5C (top), we can clearly observe the fluctuations in n_b^{pred} increasing with b. Here, we simply estimated n_b^{pred} from the binned data. However, fluctuations can be reduced by estimating firing rates on the original resolution h and using equation 3.4 to obtain the occupation probability at bin size bh. The dependence of the joint-surprise (see Figure 5, bottom row) on the bin size is similar to the above-described dependence on the rate (cf. Figure 4). In the absence of injected coincidences, S fluctuates around 0 (see Figure 5A). For injected coincidences, S decreases with increasing bin size. The lower the injection rate is, the sooner S starts to decrease and the faster it decays: for $\lambda_c = 0.5\text{s}^{-1}$, joint-surprise values start to fall below the 0.01 significance level at $b = 3$ (see Figure 5B), while for $\lambda_c = 1.0\text{s}^{-1}$, significance is maintained up to about $b = 6$ to 10 (see Figure 5C). Again, the decline in S is controlled by the decreasing ratio $(n_b^{\text{emp}} - n_b^{\text{pred}})/n_b^{\text{pred}}$. The similarity between the dependences of S on spike rate and on bin size is not surprising, considering that binning has the net effect of an apparent increase in firing probability, limited by the additional effect of clipping.

3.3 Detection of Near-Coincidences. In a next step, we investigate whether it is also possible to detect noisy (i.e., imprecise) coincidences. This question arises naturally, since neurons are usually considered to exhibit some degree of "noise" or uncertainty in the timing of their action potentials. Note, however, that the degree of this temporal noise has long been questioned (e.g., Abeles, 1983) and is still under debate, (e.g., Mainen & Sejnowski, 1995; Shadlen & Newsome, 1998; Diesmann et al., 1999). While keeping both the independent background rate and the injection rate constant, we increase the temporal jitter of the injected near-coincident events stepwise from 0 to 5 ms, such that in each case, the difference in spike times is uniformly distributed within the chosen jitter range. The question is whether, by choosing an appropriate binning grid, we can improve the detection of such near-coincident events. To this end, we analyze the simulated data with varying bin sizes and for each bin size compute the joint-surprise.

Figure 6 shows the results for a background rate of $\lambda = 30\text{s}^{-1}$ and a rate of injected near-coincidences $\lambda_c = 2\text{s}^{-1}$. Each of the curves in Figure 6A represents data with a particular temporal jitter s, analyzed with a bin size bh increasing from 1 ms to 10 ms. Values of S are averages of 100 repetitions of the simulation experiment at constant parameters. Each curve exhibits a global maximum (marked by an asterisk) at a bin size b_* close to the magnitude of the jitter of the injected coincidences; b_* is shown as a function of temporal jitter in Figure 6B. Indeed, the maxima occur at the bin size that in a given simulation just covers the maximal jitter (e.g., spikes with a maximal time difference of $s = 1$ are covered by a bin size spanning two time steps of the original time resolution: $b = 2$). Numerical analysis of an analytical

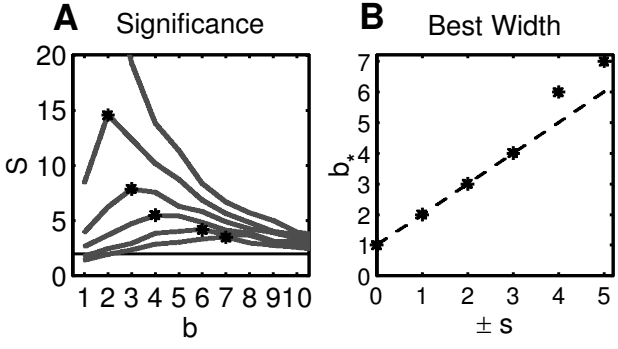

Figure 6: Detection of near-coincidences for different degrees of coincidence precision. Two parallel spike trains were generated with background rates $\lambda = 30\text{s}^{-1}$ the rate of the injected coincidences was $\lambda_c = 2\text{s}^{-1}$, for $T = 10^5$ time steps, $h = 1$ ms. The temporal jitter of coincident events was varied from $s = 0$ to $s = 5$ time steps. Each simulation was repeated 100 times, and data were analyzed for the number of observed coincidences by varying the analysis bin size from $b = 1$ to $b = 10$, and compared to the expected coincidence count assuming independence. (A) Each curve shows the resulting average joint-surprise as a function of the analysis bin size for a given temporal jitter. The top curve shows the results for $s = 0$, the bottom curve for $s = 5$, intermediate scatters in between (using the maxima as reference). Maxima of the curves are marked by an asterisk. (B) Optimal bin width b_* for detecting excess coincidences as a function of temporal jitter, theoretical curve indicated by dashed line.

description of the situation (Grün et al., 1999) shows that maxima are located at $b_* = s - 1$. The fact that in the simulation results in Figure 6B, the maxima for $s = 4$ and 5 occur at a larger bin size is due to fluctuations remaining in the averaged S. For bin sizes smaller than the scatter width, S increases with bin size since for more and more near-coincidences, the constituting spikes fall into a common bin. At bin sizes larger than the coincidence accuracy, the rate at which the number of excess coincidences grows drops, and the probability that an injected coincidence is detected slowly reaches saturation. Thus, S is bound to decrease again, because the expected coincidence count assuming independence continues to grow approximately linearly. The joint-surprise curves for finite temporal jitter s approach the curve for perfect coincidences $s = 0$ from below. The comparison of different joint-surprise curves shows that the higher the temporal jitter (i.e., the lower the coincidence accuracy) is, the lower the joint-surprise is. Hence, for a given b, the number of near-coincidences that can be detected increases with decreasing temporal jitter.

3.4 Multiple Parallel Processes. When the number of simultaneously observed neurons N is increased, the variety of coincidence patterns grows

strongly, due to the nonlinear increase in combinatorial possibilities. Each complexity ξ (i.e., a spike pattern with ξ 1s, $N - \xi$ 0s) can in principle occur in $\binom{N}{\xi}$ variations. On the other hand, the occurrence of higher-order constellations depends in a nonlinear fashion on the rates. The probability for a pattern with complexity ξ to occur among N neurons, all firing independently with probability p, is given by $p^{\xi} \cdot (1-p)^{N-\xi}$. For low firing probabilities ($p \ll 1$), this can be approximated by p^{ξ}. By the combination of these two effects, constellations of high complexity are actually expected to occur rarely. For low firing probabilities, such as $p = 2 \cdot 10^{-2}$, the expected count for a coincidence pattern of complexity $\xi = 3$ (assuming a total number of observation time steps $T = 10^5$) is of the order of 1 or less, and even less for higher complexities (see Figure 7B, top). For higher firing probabilities, this expectation is shifted to larger values. Consider a pattern of complexity 4, with other parameters as above. The expected coincidence count now is $n^{\text{pred}} = 0.016$; the probabilities of finding 0, 1, or 2 coincidences are approximately $\psi(0, n^{\text{pred}}) = 0.9841$, $\psi(1, n^{\text{pred}}) = 0.0157$, and $\psi(2, n^{\text{pred}}) = 0.0001$. Here, the discrete nature of the Poisson distribution is fully exhibited. Almost all the mass is at a single outcome (0). The joint probabilities of outcomes 1 and 2 are $\Psi(1 \mid n^{\text{pred}}) = 0.0159$ and $\Psi(2 \mid n^{\text{pred}}) = 0.0001$, respectively. Thus, at an α-level of 0.01, the occurrence of two coincidences is already significant and would still be significant for much lower α values. If the occurrence of 2 or more coincidences than expected is significant for almost any significance level, our measure is obviously susceptible to fluctuations. The significance of the spike constellation in a particular experiment cannot be determined precisely. The obvious and standard cure to this problem is to collect more data for such an experimental situation, shifting the distribution of the coincidence counts for patterns of high complexity to larger expectation values, where the discrete nature of the distribution is of less importance.

As a result of the above discussion, high ξ constellations, if occurring at all, are typically accompanied by high joint-surprise values (cf. Figure 7B, bottom). It is therefore not surprising that in simulations where we varied the complexity of the injected coincidence patterns from $\xi = 2$ to 6 (while keeping the number of processes ($N = 6$), the background rate ($\lambda = 20\text{s}^{-1}$) and the injection rate ($\lambda_c = 1\text{s}^{-1}$) constant), all coincidences of complexity ≥ 3 were detected with high significance (see Figure 7B, bottom). Moreover, the measured coincidence counts for $\xi \geq 3$ are close to the expectation for the injected coincidence $\lambda_c hT = 100$ (see Figure 7B, top). For complexity 2, the coincidence count is higher, because we get contributions from the background rate $(\lambda h)^2 T = 40$. This contribution is rapidly vanishing for higher complexities (e.g., $\xi = 3$, $(\lambda h)^3 T = 0.8$).

Similar results were obtained when we increased the number of independent processes N (from 2 to 12), while keeping the complexity of injected coincidences constant ($\xi = 2$, Figure 7A). Here, injection means that

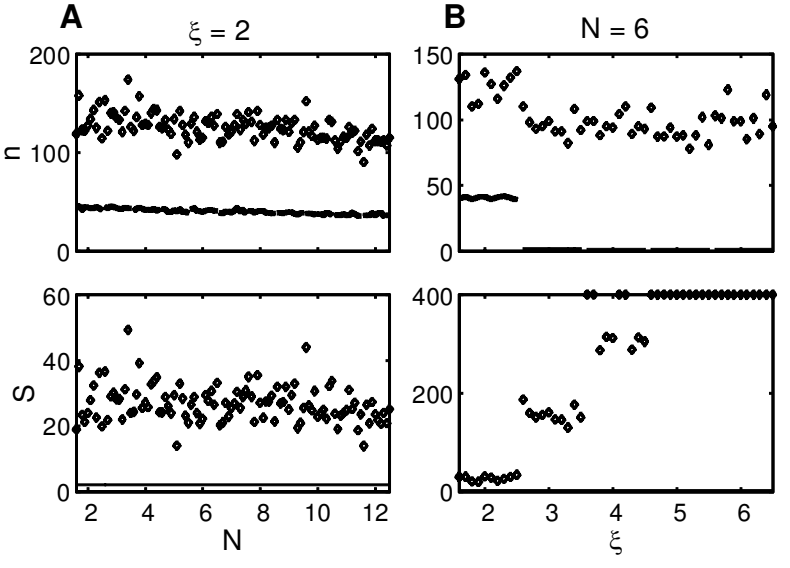

Figure 7: Complexity of joint spike patterns. (A) The number of processes into which a pair of coincidences (complexity $\xi = 2$) was injected was varied from 2 to 12. The rate of the independent processes was $\lambda = 20\text{s}^{-1}$, and the injection rate was $1\ \text{s}^{-1}$ ($T = 10^5$, 10 repetitions). The diamonds in the upper graph show the number of occurrences of the coincidence patterns [110], [1100], [11000], and so on, with the number of zeros depending on the number of processes. The expected counts are shown as solid lines. The lower graph shows the joint-surprise for the corresponding pairs of measured and expected counts; the horizontal line marks the significance level of 0.01. (B) The number of processes was kept constant ($N = 6$), as were their rates (parameters as in A), but the complexity of the injected coincidences was varied from 2 to 6. Thus, the pattern looked for was [110000], [111000], and so on, respectively. The measured counts of the coincidence pattern are displayed as diamonds, the expected counts as solid lines. The latter values cannot be distinguished from 0 for $\xi > 3$ in this graph, because values become very small. The corresponding joint-surprise (bottom panel) was therefore very high (clipped here to an arbitrary value of 400 for visualization).

simultaneous spikes are added to ξ of the N parallel spike trains, without affecting the $N - \xi$ remaining ones. It turns out that the joint-surprise of the ξ constellation (i.e., ξ 1s and $N - \xi$ 0s) at the given firing rates is practically independent of N. There is a small decrease in the number of occurrences of this particular pattern, because with increasing N, more patterns containing the two spikes as a subpattern become available. However, this effect does not seriously affect the detectability of the injected

coincidences. The situation changes when massively parallel data are examined, and patterns of higher complexity become typical. Let the two neurons under consideration be accompanied by 98 other neurons, other parameters as above. The probability that at least 1 of the 98 neurons contributes a spike to the coincidence is $\sum_{k=1}^{98} \binom{98}{k} (\lambda h)^k (1 - \lambda h)^{98-k}$, which is $1 - (1 - \lambda h)^{98} \approx 0.86$.

We conclude that to decide on the empirical relevance of coincidences of higher complexities ($\xi \geq 3$), given a moderate amount of data, it is advisable to set additional criteria, for example, by requiring a minimum absolute number of occurrences (see also Abeles, Bergman, et al., 1993; Martignon, Laskey, Deco, & Vaadia, 1997; Martignon et al., 2000).

4 False Positives

Up to now, we have studied the sensitivity of our method by exploring under which conditions excess coincident events are detectable. However, while striving for high sensitivity (a low fraction of false negatives), we simultaneously need to ensure an appropriately high degree of specificity (a low fraction of false positives). Such false positives are the result of incorrectly assigning the label "excess coincidences" to an experiment where they in fact are not in excess. Thus, we have to establish conditions under which we reach a compromise between a sufficient degree of sensitivity and an acceptable degree of specificity. Therefore, we now analyze various sets of simulated data, with the combined requirement of attaining a high level (90%) of detection (only 10% false negatives), while securing a low level (10%) of false positives. As in the preceding sections, the simulations are described by biologically relevant parameters, varied over a physiologically realistic regime. 100 independent experiments were performed for each parameter value; from these, the percentage of experiments that crossed a certain threshold level on the joint-surprise was evaluated. This threshold level α was varied in equidistant steps to cover the range of joint-surprise values between -15 and $+15$.

4.1 Influence of the Firing Rate. In the first step, we kept the number of independent processes constant ($N = 2$) and varied the rate of the processes. We found that for constellations of complexity 2, the percentage of false positives is practically independent of the background rates (see Figure 8A, left). This is not surprising, because if the rates of the underlying processes were known, and therefore the expected number of coincidences assuming independence n^{pred} could be determined without error, α would represent the percentage of experiments passing S_α. The above result ensures that for the parameter regime tested, determination of firing rates from the data does not cause dramatic deviations of the percentage of false positives from the theoretical level α.

By contrast, the sensitivity for detecting excess coincidences shows a clear dependence on background rates. At low rates, it is very high, but it decreases—rapidly at first, more slowly later—with increasing background rate (see Figure 8A, middle). At background rates above $\lambda = 60\text{s}^{-1}$, the threshold for detecting the injected events has decayed to about $\alpha = 0.05$. Combining these two observations in a single graph, we obtain the intersection range of the joint-surprise, necessary to obtain both maximally 10% false positives and minimally 90% sensitivity (the white area in Figure 8A, right). For low α, this region is bounded by an approximately straight vertical line at $\alpha = 0.05$; the lower boundary of the permissible significance measure is approximately independent of the background rate. The upper bound, however, is clearly curved: the threshold needed for reliable detection decreases with increasing background rate, reaching a level of only 0.05 at $\lambda = 60\text{s}^{-1}$. Thus, the higher the rate is, the narrower is the bandwidth of α-values permissible to detect excess coincident events selectively and sensitively.

4.2 Influence of the Number of Parallel Processes. Next, we varied the number of independent processes (from 2 to 12) while keeping the rates constant ($\lambda = 20\text{s}^{-1}$). For each number of processes, the fractions of false positives and false negatives were evaluated at different threshold levels. We found that the fraction of false positives increased with decreasing threshold and in the given range was independent of the number of processes involved (see Figure 8B, left). Moreover, the sensitivity for excess coincidences (shown for complexity 2 at coincidence rate of 1 s^{-1} in Figure 8B, middle) was independent of the number of processes as well. The intersection range of the joint-surprise, necessary to obtain maximally 10% false positives and maximally 10% false negatives, is shown in white in Figure 8B (right panel). Observe the wide parallel band for selective and sensitive detection, independent of the number of observed processes. If more restrictive criteria (fewer false positives and/or fewer false negatives) are adopted, the band becomes accordingly smaller (not shown here).

4.3 Influence of Pattern Complexity. Higher-order coincidences (coincidences with high complexity ξ) are rarely found in data with low firing rates and limited numbers of observation time steps (see also section 3.4). Figure 8C (left) illustrates that there are hardly any false positives for complexities 4 or higher, even for threshold levels of $\alpha > 0.5$. Let n_α represent the smallest n for which $\Psi(n_\alpha \mid n^{\text{pred}}) < \alpha$. Because of the discrete nature of the distribution of coincidence counts ψ (see section 3.4), $\Psi(n_\alpha \mid n^{\text{pred}})$ can actually be much smaller than α (see the example in section 3.4). If n^{pred} is exact, $\Psi(n_\alpha \mid n^{\text{pred}})$ actually is the fraction of false positives expected. Therefore, the percentage of false positives can be much smaller than α. This does not contradict the fact that if such coincidences occurred, its joint-surprise would indicate high significance. False positives of lower complexity (up to

3) do show up for threshold levels α below 0.5, but their fraction decreases with pattern complexity. The situation is even more clear-cut for the case of false negatives (see Figure 8C, middle). The detection of injected coincidences is practically 100%. Thus, the intersection graph of the joint-surprise for fewer than 10% false positives and fewer than 10% false negatives (see Figure 8C, right) shows noncompliance for negative values of S_α and $\xi < 4$.

5 Discussion

We described a new method to analyze simultaneously recorded single-unit spike trains for signs that (some of) the observed neurons are engaged in a cell assembly. We adopted a widely used operational definition, defining common assembly membership on the basis of near-simultaneity of the joint spike activity of the observed neurons (Abeles, 1982a; Gerstein et al.,

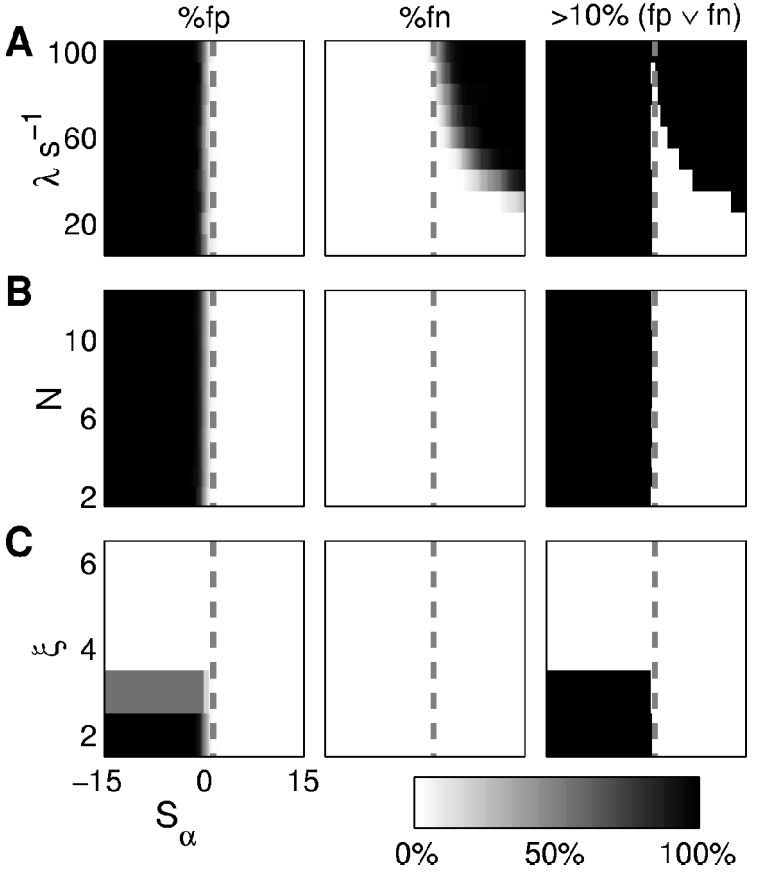

1989). The simultaneous observation of spiking events from N neurons was described by the joint process of N parallel spike trains. By appropriate binning, this was transformed to an N-fold (0,1)-process, a realization of which is represented by a sequence of N-dimensional activity vectors (instances of coincidence patterns) describing the various (0,1)-constellations that occurred across the recorded neurons. Under the null hypothesis of independently firing neurons, the expected number of occurrences of any coincidence pattern and its probability distribution could be calculated analytically on the basis of the single-neuron firing rates. The degree of deviation from independence among the neurons was evaluated by comparing the theoretically expected counts with their empirical counterparts. In order to test the significance of deviations from expectation, we developed a new statistical measure: the joint-surprise. For any coincidence pattern, the joint-surprise measures the probability of finding the observed number of occurrences (or an even larger one) by chance. Those coincidence patterns that violate the null-hypothesis of independence define potentially interesting occurrences of unitary joint events. The neurons that contribute a spike to the significant coincidence pattern are considered a subset of the neurons currently engaged in assembly activity.

To calibrate the new method and test its performance, we applied it to simulated data sets in which different physiological and analysis parameters were varied in systematic fashion. We used independent Poisson processes

Figure 8: *Facing page*. Selectivity and sensitivity as a function of firing rate (A), number of neurons (B), and pattern complexity (C). In the left column, the percentage of false positives (fp), that is, $1 -$ selectivity, is calculated using independent data sets, without injected coincident events. The percentage of false negatives (fn), that is, $1 -$ sensitivity, for injected events as a function of the threshold level S_α (abscissa) is shown in the middle column. The overlap regions of maximally 10% false positives and maximally 10% false negatives are indicated in white in the right column. (A) The percentage of false positives and false negatives of pair coincidences within spike data of two parallel processes. The rates of both independent processes λ were identical and increased from 10 s^{-1} to 100 s^{-1} in steps of 10 s^{-1} (ordinate). In the middle and right panels, coincident events of complexity 2 were injected (1 s^{-1}) into the spike data. For each rate, the experiment was repeated 100 times, $T = 10^5$, $h = 1$ ms. The density plots (gray-level coding as indicated) represent the percentage of experiments that crossed the threshold level S_α (fp, left column) or remained below it (fn, middle column), respectively. (B) The percentage of fp and fn for coincidences of complexity 2 for varying numbers of processes N (ordinate), increasing from 2 to 12 (firing rate held constant at 20 s^{-1}, coincidences injected at rate 1 s^{-1} into 2 of the N processes). Display and other parameters as in A. (C) The percentage of fp and fn for coincidences of varying complexity (ordinate) in a fixed number of processes ($N = 6$). Display and other parameters as in A. For orientation, the threshold level for $\alpha = 0.05$ is indicated by a dashed line in all plots.

to generate control data at various firing rates. The degree of interdependence of the surrogate data was controlled by injecting coincident spiking events at different rates, timing precision, and neuron composition. Specifically, we measured the sensitivity (the probability not to generate false negatives) and the specificity (the probability not to generate false positives) of the method and determined its dependence on various physiological parameters. Overall, the method proved to be both highly sensitive and highly specific to detect the presence of even weak signs of coincident spiking. Moreover, the method is only moderately sensitive to wide-range variations of the tested parameters, largely covering the physiologically relevant regime encountered in cortical neuron recordings. Thus, unitary event analysis provides a simple measure to test for the presence of excess coincident spiking events in experimental data. Since the method takes into account the firing rates of the observed neurons, results from different experiments and/or recordings may be compared. The principal ingredient of the method is the joint-surprise. It provides a convenient measure of the probability that the number of coincident spiking events represents a chance constellation. One may stop at this point and use the resulting probabilities (e.g., by comparing them across different experimental or behavioral conditions) as a means to assess the functional relevance of synchronous spiking. Another way to proceed, explored in this article, is to adopt a common approach in statistics by imposing a threshold level on the joint-surprise function and to focus on the data where this minimum significance level (e.g., $\alpha = 0.05$ or 0.01) was surpassed. In doing so, selections from the data are highlighted as potentially interesting regarding the presence of excess coincident spiking events. We referred to these events as unitary events, marking highly unexpected joint spike constellations. Their neuronal composition, as well as the moments at which they occur, may provide information about the underlying dynamics of assembly activation. It is worthwhile to point out that our method does not allow us to distinguish on an individual spike basis which one is an excess event and which is not. Hence, all instances of a significant coincidence pattern are marked. Nevertheless, unitary events may well occur inhomogeneously distributed over the time interval studied, revealing a potentially interesting time structure in relation to the experiment that is not present in the original stationary firing rates.

We have formulated the null-hypothesis in terms of statistical independence. In cases where a specific time structure within a single spike train is of interest (e.g., Legendy & Salcman, 1985; Dayhoff & Gerstein, 1983), independence is often formulated as the assumption that the neuronal spike train is a realization of a Poisson process. In cases where parallel processes are tested for spatio and/or temporal patterns (as in our case), often independent Poisson processes are assumed—that is, both independence within the spike trains and independence between them (Palm et al., 1988; Abeles & Gerstein, 1988; Aertsen et al., 1989; Prut et al., 1998). Physiological data, however, often violate the Poisson assumption, and it

is not yet clear how to correct for that in a general (i.e., model-free) manner. One option is to make different assumptions about the nature of the underlying point process, for example, to assume that it is a renewal process (Cox & Isham, 1980) or, more specifically, a γ -process (e.g., Pauluis & Baker, 2000; Baker & Lemon, 2000). We have tested the influence of violations of the Poisson assumption on the occurrence of false positives using γ -processes (see appendix B). Results from our parametric study, where the structure of the point processes was varied from bursty to regular firing, indicate that the unitary event analysis method is quite robust against such violations. Another option, which we are currently exploring, is a bootstrap-type method, shuffling the spike trains across trials to generate surrogate data from which one can estimate the expected numbers of the various constellations quasi-empirically (Pipa, Singer, & Grün, 2001). By this procedure, the temporal structure of the individual spike trains is taken into account, and an explicit hypothesis about the generation processes need not be made. Another aspect of extending the formulation of the null-hypothesis is to take into account correlations among subsets of neurons. In this context, a promising new approach proposed recently is to extend the null-hypothesis of independence to incorporate interactions among subsets of the neurons contributing spikes to a given coincidence pattern (Martignon, von Hasseln, Grün, Aertsen, & Palm, 1995; Martignon et al., 1997, 2000).

Constellations of complexity higher than 2 in independent multiple parallel processes are relatively rare. However, if they occur, they are very likely to be detected as false positives in data sets of finite length (see section 3.4; Roy et al., 2000). In order to account for that, it is advisable to apply an additional test at a meta-level, for example, by requiring a minimal absolute number of occurrences of the high-complexity event or by applying an additional statistical test (Prut et al., 1998). Also here, bootstrap techniques may be invoked (e.g., Nadasdy, Hirase, Czurko, Csicsvari, & Buzsaki, 1999) to provide additional means to differentiate false positives from true positives in such regimes of relatively rare occurrences.

Another source for false positives is the violation of the assumption of stationarity. The firing rates, measured by averaging over time (and trials) and serving as the basis to test the null-assumption, may not reflect the instantaneous behavior. Particularly in regions with a higher-than-average rate, unitary events may be detected by our method for incorrect reasons (for related problems with cross-correlation measures, see, e.g., Brody, 1999a, 1999b). Unfortunately, however, a strict requirement of stationarity may sometimes disqualify a large portion of the experimental data, especially from awake, behaving animals. Therefore, a more promising approach is to adopt techniques that enable us to make reliable estimates of the instantaneous firing rates (Nawrot, Aertsen, & Rotter, 1999; Pauluis & Baker, 2000). Giving up the concept that neuronal spiking is driven by a (potentially time-dependent) intensity function, the significance test can also be based

on counting statistics, thereby removing the problem of rate estimation from experimental data (Gütig et al., in press).

The method of unitary event analysis bears clear relations to the dynamic analysis of cross-correlation, as exemplified, for example, in the JPSTH (Aertsen et al., 1989). It presents an extension, in that it enables us to analyze more than two neurons at a time, and a restriction, by focusing on coincident events only. In principle, the method could also accommodate any specific arrangement of coincidence delays unequal to zero. However, the combinatoric problems associated with exploring all possible such arrangements are beyond our present capabilities. The synfire model (Abeles, 1991) has prompted scientists to search specifically for spatiotemporal firing patterns in multiple single-neuron spike trains (Abeles & Gerstein, 1988; Abeles, Bergman, et al., 1993; Villa & Abeles, 1990; Prut et al., 1998; Date, Bienenstock, & Geman, 1998). However, in contrast to the method of Prut et al. (1998), unitary event analysis focuses on spatial patterns. Binning provides a general and straightforward mechanism to control the amount of temporal jitter allowed in the definition of a coincidence. It is applicable to N parallel processes. Unfortunately, for coincidences with large temporal jitter, sensitivity is reduced due to the fission of coincidences at the binning grid (see section 3.2; Grün et al., 1999). For $N = 2$, methods have been developed to detect near-coincidences without the need of binning (Grün et al., 1999; Pauluis & Baker, 2000). However, no method currently exists for $N > 2$. We are exploring the detection of near-coincidences in large numbers of parallel processes without discretization of time (Grün & Diesmann, 2000).

One important issue remains to be solved before we can apply this framework to physiological data and study neuronal assembly dynamics in relation to stimuli and behavioral events. Until now, we have considered only the case of neurons firing at a stationary rate and with stationary coincident activity among them. Physiological data, however, are usually not stationary. Firing rates vary considerably as a function of time, particularly when the animal is presented with adequate stimuli or is engaged in a behavioral task. A second type of nonstationarity is that coincident firing itself may be nonstationary for example, by being time-locked to a stimulus or behavioral event even if the rates of the neurons are constant (Vaadia et al., 1995). Since our analysis so far derives its measures globally from the entire observation interval, the time-locked occurrence of coincidences might be overlooked. In the companion article in this issue, we address both types of nonstationarities and extend our theoretical framework accordingly.

Appendix A: Notation

$\mathcal{T}$	temporal duration of observation interval, $[\mathcal{T}]$ = unit of time
h	time resolution of data, $[h]$ = unit of time
T	temporal duration of observation interval in units of h, $[T] = 1$
M	number of trials

v_i	(0,1)-sequence of neuron i
N	number of simultaneously observed neurons
$\mathbf{v}(t)$	coincidence pattern at time step t, N-dimensional vector
$\mathbf{v}^k$	coincidence pattern k, N-dimensional vector
m	number of possible patterns
$\xi(\mathbf{v}^k)$	complexity of $\mathbf{v}^k$
n	general coincidence count
n_k^{emp}	empirical coincidence count of $\mathbf{v}^k$
n_k^{pred}	expected coincidence count of $\mathbf{v}^k$
P	general probability in expressions like $P(k \geq 1)$
p_i	occupation probability for neuron i
P_k	probability of coincidence pattern $\mathbf{v}^k$
ψ	distribution of coincidence counts
Ψ	joint-p-value
S	joint-surprise
α	significance level
λ	background firing rate, $[\lambda] = 1/\text{unit of time}$
λ_c	coincidence rate, $[\lambda_c] = 1/\text{unit of time}$
b	bin size in units of h, $[b] = 1$
T_b	number of time steps after binning, $[T_b] = 1$
p_b	occupation probability after binning
s	temporal jitter of injected coincidences in units of h, $[s] = 1$
MD_k	mutual dependence of $\mathbf{v}^k$; see appendix C
$\text{MD}(t)$	time-resolved mutual dependence

Appendix B: Violation of the Assumption of Poissonian Spike Trains

In order to test how sensitive the unitary event analysis method is to a violation of the assumption of Poisson spike trains, we conducted the following experiment: Independent parallel spike trains ($N = 2$) were modeled as γ-processes and analyzed for the occurrence of significant coincident events—false positives (similar to section 4). A γ-process allows us to vary the spike train structure from "burstiness" to regular spiking by variation of a single parameter only: the "shape" parameter γ. γ-processes belong to the class of renewal processes and can be simulated by successively drawing interspike intervals from the interval distribution

$$f(\tau) = \lambda \cdot e^{-\lambda\tau} \cdot \frac{(\lambda\tau)^{\gamma-1}}{\Gamma(\gamma)}. \tag{B.1}$$

For $\gamma = 1$ the spike train is Poissonian (coefficient of variation (CV) = 1). If γ is chosen < 1, the resulting spike train exhibits clusters or bursts of spikes, leading to a high variability of the interspike intervals (CV > 1). By contrast, if γ is chosen > 1, the spike train is more regular; the higher the γ is, the smaller is the variability of the interspike intervals ($CV < 1$).

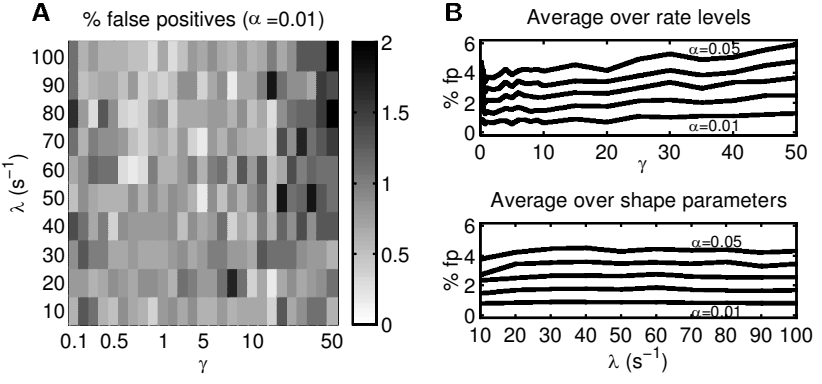

Figure 9: False positives in non-Poissonian spike trains. Two parallel spike trains of duration $T = 100$ s and time resolution $h = 1$ ms were simulated as independent γ -processes with parameters rate λ and shape factor γ . λ was varied from 10 to 100 s^{-1} in steps of 10 s^{-1}, and the shape factor γ was varied between 0.1 and 50, in steps of 0.1 between 0.1 and 1, up to 10 in steps of 1, and above in steps of 5. For each parameter constellation, the simulation was repeated 1000 times; the percentage of cases showing significant outcomes at given significance levels are derived as false positives (fp). (A) The matrix illustrates the percentage of false positives in gray code as a function of shape factor (horizontal) and given rate parameter (vertical) for a significance level $\alpha = 0.01$. Note that the resulting rate may differ from the given rate parameter, since for shape factors $\gamma < 1$, a relatively large number of spikes occur with interspike intervals $\leq h$, which are clipped to one spike per time resolution bin in the simulation process. The larger the given rate and the smaller γ , the larger the reduction in rate (at $\lambda = 100s^{-1}$ and $\gamma = 0.1$ about 50%). (B) Percentage of false positives as a function of γ averaged over all rate levels (top) and as a function of rate parameter λ averaged over all shape factors (bottom) displayed for various significance levels $\alpha = 0.01, 0.02, \ldots, 0.05$.

For $\gamma \to \infty$, the process approaches a clock process, with a fixed value for the interspike interval. Thus, by varying the shape factor from 0.1 to 50, we covered a wide range of variability of experimentally observed spike trains (e.g., Softky & Koch, 1993; Baker & Lemon, 2000; Nawrot, Riehle, Aertsen, & Rotter, 2000).

For the significance test, the same procedure was used as introduced for the Poissonian spike trains: a Poisson distribution with its mean set to the expected number of coincidences (see equations 2.3 and 2.9). Two parameters were systematically varied in the simulations: the rate parameter λ of the processes and the shape factor γ . For each parameter constellation, the simulation of duration $T = 100s$ was repeated 1000 times, and the percentage of cases showing significant outcomes was derived. Figure 9A illustrates

the percentage of false positives in gray code as a function of shape factor (horizontal) and rate parameter (vertical) for a significance level $\alpha = 0.01$. Observe that the percentage of false positives varies between 0% and 2%—in a range around the expected value given the applied significance level of 1%. The matrix does not appear to be clearly structured but shows a weak tendency for higher percentages of false positives (2%) with increasing rate and shape factor.

The projections (and averages) of the results onto the shape axis (see Figure 9B, top) and on the rate axis (see Figure 9B, bottom) show that an increasing rate does not vary the number of false positives but with increasing shape factor, the number of false positives increases slightly, which is somewhat stronger for less strict significance levels ($\alpha = 0.02 \cdots 0.05$).

In summary, we conclude that the unitary event analysis method behaves quite robustly with respect to the significance level α against a violation of the Poisson assumption, realized here as γ -processes.

Appendix C: Mutual Dependence

A different approach to detect dependencies in parallel spike data is to use a measure related to the general framework of information theory: *mutual dependence*, derived from the mutual information and redundancy (for details, see Grün, 1996). For each particular activity constellation $\mathbf{v}^k$, mutual dependence MD_k is defined in terms of the joint-probability P_k^{pred} expected under the null-hypothesis (see equation 2.3) and its empirical counterpart,

$$P_k^{\mathrm{emp}} = \frac{n_k^{\mathrm{emp}}}{T}, \tag{C.1}$$

by

$$\mathrm{MD}_k = \ln \frac{P_k^{\mathrm{emp}}}{P_k^{\mathrm{pred}}}. \tag{C.2}$$

Thereby, we obtain:

$$\begin{array}{llll} \text{if} & P_k^{\mathrm{emp}} < P_k^{\mathrm{pred}} & \text{then} & \mathrm{MD}_k < 0: \quad \text{“negative” dependence} \\ \text{if} & P_k^{\mathrm{emp}} = P_k^{\mathrm{pred}} & \text{then} & \mathrm{MD}_k = 0: \quad \text{independence} \\ \text{if} & P_k^{\mathrm{emp}} > P_k^{\mathrm{pred}} & \text{then} & \mathrm{MD}_k > 0: \quad \text{“positive” dependence.} \end{array} \tag{C.3}$$

Hence, any deviation of MD_k from 0 will indicate deviations from the null-hypothesis of independence for the corresponding activity constellation $\mathbf{v}^k$. Note that mutual dependence is a time-averaged measure over the entire duration of the spike trains under observation. We can make this into

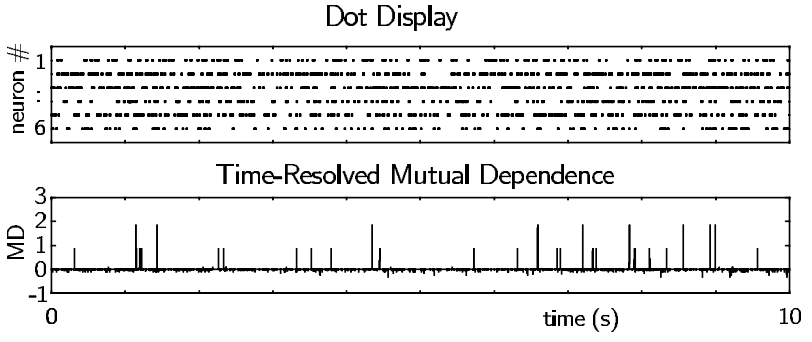

Figure 10: Time-resolved mutual dependence. The dot display (top) and the time-resolved mutual dependence (bottom) are shown for a simulated data set, into which coincident spikes were injected (same data as in Figure 3B) . In contrast to Figure 3B, spike data of the trials are concatenated and, individually for each neuron, represented as a single continuous series of dots.

a "local" time measure, however, by replacing each individual vector $\mathbf{v}^k$ at the points in time where it occurs t_j^k, $j \in \{1, \ldots, n_k^{\text{emp}}\}$ by the associated mutual dependence value MD_k. This leads to a time-varying function: the *time-resolved mutual dependence* $\text{MD}(t)$:

$$\text{MD}(t) = \sum_{k=1}^{m} \sum_{j=1}^{n_k^{\text{emp}}} \text{MD}_k \cdot \delta(t - t_j^k). \tag{C.4}$$

The delta function in equation C.4 selects the MD value corresponding to the coincidence pattern occurring at the time of interest. The resulting time series describes the individual contributions to the MD in the course of time. The result is a discontinuous, "peaky" function of time, as shown in Figure 10 for a simulated data set with injected coincident events. The amplitudes, ranging from negative to positive values, typically vary strongly from one time step to the next. Positive amplitudes tend to have higher values than negative ones and pop out from small fluctuations around 0. Positive peaks "point" to spike constellations for which the probability of occurrence is higher than expected, assuming independent processes. Negative peaks "point" to spike constellations with probability of occurrence lower than expected. Thus, the time-resolved mutual dependence may be interpreted as a "dynamic pointer" to instances of joint spike constellations representing conspicuous deviations from independence.

A comparison of the performance of MD to the joint-surprise with regard to false positives and false negatives (cf. section 4) revealed that the

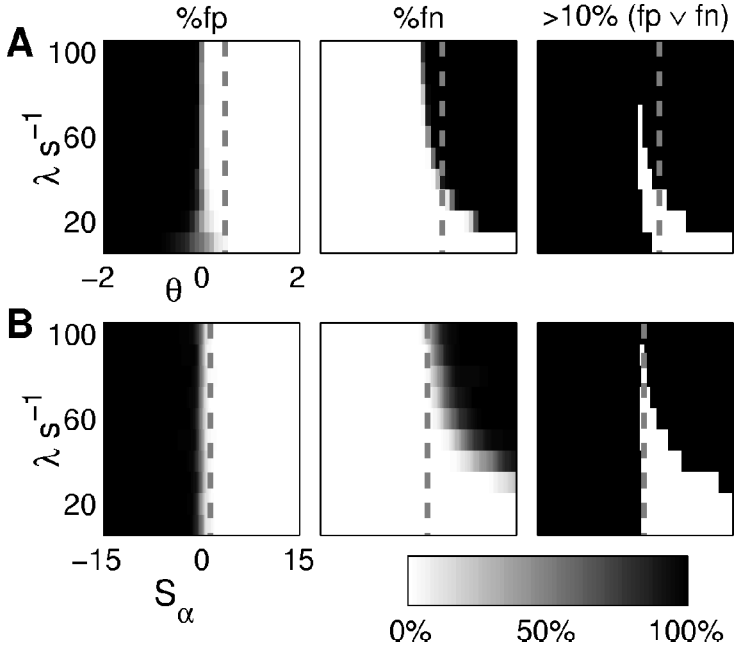

Figure 11: (A) Selectivity and sensitivity of the mutual dependence for pair coincidences injected into two parallel processes as a function of firing rates. (B) Results for the joint-surprise for comparison. The percentage of false positives (fp: left column), false negatives (fn: middle column), and the resulting overlap of maximum 10% fp and maximum 10% fn (right column). The thresholds on the MD were varied from $\theta = -2$ to 2 in equidistant steps. The dashed line indicates the MD-value corresponding to S_α ($\alpha = 0.05$) for background rates $\lambda = 10\text{s}^{-1}$. Further details as in Figure 8.

MD measure, in contrast to the joint-surprise, strongly depends on the firing rates of the neurons involved (see Figure 11). This dependence expresses itself in the curved shape of the sensitivity-selectivity overlap region (the white area in Figure 11A, right). As a result, different significance thresholds would be required for different firing rates. Thus, to obtain an adequate performance of the MD, the threshold needs to be adjusted, point by point, to the associated rates. Evidently, this is unpractical, considering that the observed processes typically have different individual firing rates. In addition, rate dependence poses problems when comparing data from different experiments. For the above reasons, we do not pursue this measure further here; more details and results of application to neuronal data can be found in Grün (1996).

Acknowledgments

We thank Moshe Abeles, George Gerstein, and Günther Palm for many stimulating discussions and help in the initial phase of the project. We also thank Robert Gütig, Stefan Rotter, and Wolf Singer for their constructive comments on an earlier version of the manuscript for this article. This work was partly supported by the DFG, BMBF, HFSP, GIF, and Minerva.

References

Abeles, M. (1982a). *Local cortical circuits: An electrophysiological study*. Berlin: Springer-Verlag.

Abeles, M. (1982b). Quantification, smoothing, and confidence limits for single-units' histograms. *J. Neurosci., 5*, 317–325.

Abeles, M. (1982c). Role of cortical neuron: Integrator or coincidence detector? *Israel J. Med. Sci., 18*, 83–92.

Abeles, M. (1983). The quantification and graphic display of correlations among three spike trains. *IEEE Trans. Biomed. Eng., 30*, 236–239.

Abeles, M. (1991). *Corticonics: Neural circuits of the cerebral cortex*. Cambridge: Cambridge University Press.

Abeles, M., Bergman, H., Margalit, E., & Vaadia, E. (1993). Spatiotemporal firing patterns in the frontal cortex of behaving monkeys. *J. Neurophysiol., 70*(4), 1629–1638.

Abeles, M., & Gerstein, G. L. (1988). Detecting spatiotemporal firing patterns among simultaneously recorded single neurons. *J. Neurophysiol., 60*(3), 909–924.

Abeles, M., Vaadia, E., Prut, Y., Haalman, I., & Slovin, H. (1993). Dynamics of neuronal interactions in the frontal cortex of behaving monekys. *Conc. Neurosci., 4*(2), 131–158.

Aertsen, A., & Arndt, M. (1993). Response synchronization in the visual cortex. *Curr. Op. Neurobiol., 3*, 586–594.

Aertsen, A., Gerstein, G., Habib, M., & Palm, G. (1989). Dynamics of neuronal firing correlation: Modulation of "effective connectivity." *J. Neurophysiol., 61*(5), 900–917.

Aertsen, A., Vaadia, E., Abeles, M., Ahissar, E., Bergman, H., Karmon, B., Lavner, Y., Margalit, E., Nelken, I., & Rotter, S. (1991). Neural interactions in the frontal cortex of a behaving monkey: Signs of dependence on stimulus context and behavioral state. *J. Hirnf., 32*(6), 735–743.

Ahissar, M., E., A., Bergman, H., & Vaadia, E. (1992). Encoding of sound-source location and movement: Activity of single neurons and interactions between adjacent neurons in the monkey auditory cortex. *J. Neurophysiol., 67*, 203–215.

Baker, S., & Lemon, R. (2000). Precise spatiotemporal repeating patterns in monkey primary and supplementary motor areas occur at chance level. *J. Physiol. (Lond.), 84*, 1770–1780.

Barlow, H. B. (1972). Single units and sensation: A neuron doctrine for perceptual psychology? *Perception, 1*, 371–394.

Barlow, H. (1992). Single cells versus neuronal assemblies. In A. Aertsen & V. Braitenberg (Eds.), *Information processing in the cortex* (pp. 169–173). Berlin: Springer-Verlag.

Brody, C. D. (1999a). Correlations without synchrony. *Neural Comp., 11*, 1537–1551.

Brody, C. D. (1999b). Disambiguating different covariation types. *Neural Comp., 11*, 1527–1535.

Cox, D. R., & Isham, V. (1980). *Point processes*. London: Chapman and Hall.

Date, A., Bienenstock, E., & Geman, S. (1998). *On the temporal resolution of neural activity* (Tech. Rep.). Providence, RI: Divison of Applied Mathematics, Brown University.

Dayhoff, J. E., & Gerstein, G. L. (1983). Favored patterns in spike trains. II. Application. *J. Neurophysiol., 49*(6), 1349–1363.

DeCharms, R., & Merzenich, M. (1996). Primary cortical representation of sounds by the coordination of action-potential timing. *Nature, 381*, 610–613.

Diesmann, M., Gewaltig, M.-O., & Aertsen, A. (1999). Conditions for stable propagation of synchronous spiking in cortical neural networks. *Nature, 402*, 529–533.

Eckhorn, R., Bauer, R., Jordan, W., Brosch, M., Kruse, W., Munk, M., & Reitböck, H. J. (1988). Coherent oscillations: A mechanism of feature linking in the visual cortex? *Biol. Cybern., 60*, 121–130.

Eggermont, J. J. (1992). Neural interaction in cat primary auditory cortex II. Effects of sound stimulation. *J. Neurophysiol., 71*, 246–270.

Engel, A. K., König, P., Schillen, T. B., & Singer, W. (1992). Temporal coding in the visual cortex: New vistas on integration in the nervous system. *TINS, 15*(6), 218–226.

Feller, W. (1968). *An introduction to probability theory and its applications* (Vol. 1, 3rd ed.). New York: Wiley.

Fetz, E. E. (1997). Temporal coding in neural populations. *Science, 278*, 1901–1902.

Georgopoulos, A. P., Taira, M., & Lukashin, A. (1993). Cognitive neurophysiology of the motor cortex. *Science, 260*, 47–52.

Gerstein, G. L., Bedenbaugh, P., & Aertsen, A. (1989). Neuronal assemblies. *IEEE Trans. Biomed. Eng., 36*, 4–14.

Grammont, F., & Riehle, A. (1999). Precise spike synchronization in monkey motor cortex involved in preparation for movement. *Exp. Brain Res., 128*, 118–122.

Gray, C. M., & Singer, W. (1989). Stimulus-specific neuronal oscillations in orientation columns of cat visual cortex. *Proc. Nat. Acad. Sci. USA, 86*, 1698–1702.

Grün, S. (1996). *Unitary joint-events in multiple-neuron spiking activity: Detection, significance, and interpretation*. Thun: Verlag Harri Deutsch.

Grün, S., & Aertsen, A. (1998). Unitary events in non-stationary multiple-neuron activity. *Society for Neuroscience Abstracts, 24*, 1670.

Grün, S., Aertsen, A., Abeles, M., & Gerstein, G. (1993). Unitary events in multineuron activity: Exploring the language of cortical cell assemblies. In N. Elsner & M. Heisenberg (Eds.), *Gene—Brain—Behaviour*. Göttingen: Thieme Verlag.

Grün, S., Aertsen, A., Abeles, M., Gerstein, G., & Palm, G. (1994). Behavior-related neuron group activity in the cortex. In *Proc. 17th Ann. Meeting European Neurosci. Assoc.* Oxford: Oxford University Press.

Grün, S., & Diesmann, M. (2000). Evaluation of higher-order coincidences in multiple parallel proceses. *Society for Neuroscience Abstracts, 26*, 2201.

Grün, S., Diesmann, M., Grammont, F., Riehle, A., & Aertsen, A. (1999). Detecting unitary events without discretization of time. *J. Neurosci. Meth., 94*, 67–79.

Gütig, R., Aertsen, A., & Rotter, S. (in press). Statistical significance of coincident spikes: Count-based versus rate-based statistics. *Neural. Comp.*

Hatsopoulos, N. G., Ojakangas, C. L., Paninski, L., & Donoghue, J. P. (1998). Information about movement direction obtained from synchronous activity of motor cortical areas. *Proc. Nat. Acad. Sci. USA, 95*, 15706–15711.

Hays, W. L. (1994). *Statistics* (5th ed.). Orlando, FL: Harcourt Brace.

Hebb, D. O. (1949). *Organization of behavior. A neurophysiological theory*. New York: Wiley.

Hubel, D. H., & Wiesel, T. N. (1977). Ferrier lecture: Functional architecture of macaque monkey visual cortex. *Proc. R. Soc. Lond. B., 198*(1130), 1–59.

Johannesma, P., Aertsen, A., van den Boogaard, H., Eggermont, J., & Epping, W. (1986). From synchrony to harmony: Ideas on the function of neural assemblies and on the interpretation of neural synchrony. In G. Palm & A. Aertsen (Eds.), *Brain theory* (pp. 25–47). Berlin: Springer-Verlag.

Laubach, M., Wessberg, J., & Nicolelis, M. (2000). Cortical ensemble activity increasingly predicts behaviour outcomes during learning of a motor task. *Nature, 405*, 567–571.

Legendy, C. R. (1975). Three principles of brain function and structure. *Intern. J. Neurosci., 6*, 237–254.

Legendy, C. R., & Salcman, M. (1985). Bursts and recurrences of bursts in the spike trains of spontaneously active striate cortex neurons. *J. Neurophysiol., 53*(4), 926–939.

Mainen, Z. F., & Sejnowski, T. J. (1995). Reliability of spike timing in neocortical neurons. *Science, 268*, 1503–1506.

Martignon, L., Deco, G., Laskey, K., Diamond, M., Freiwald, W., & Vaadia, E. (2000). Neural coding: Higher-order temporal patterns in the neurostatistics of cell assemblies. *Neural Comp., 12*, 2621–2653.

Martignon, L., Laskey, K., Deco, G., & Vaadia, E. (1997). Learning exact patterns of quasi-synchronization among spiking neurons from data on multi-unit recordings. In M. Jordan & M. Mozer (Eds.), *Advances in information processing systems, 9* (pp. 145–151). Cambridge, MA: MIT Press.

Martignon, L., von Hasseln, H., Grün, S., Aertsen, A., & Palm, G. (1995). Detecting higher-order interactions among the spiking events in a group of neurons. *Biol. Cybern., 73*, 69–81.

Murthy, V. N., & Fetz, E. E. (1992). Coherent 25- to 35- Hz oscillations in the sensorimotor cortex of awake behaving monkeys. *Proc. Nat. Acad. Sci. USA, 89*, 5670–5674.

Nadasdy, Z., Hirase, H., Czurko, A., Csicsvari, J., & Buzsaki, G. (1999). Replay and time compression of recurring spike sequences in the hippocampus. *J. Neurosci., 19*(21), 9497–9507.

Nawrot, M., Aertsen, A., & Rotter, S. (1999). Single-trial estimation of neuronal firing rates. *J. Neurosci. Meth., 94*, 81–91.

Nawrot, M., Riehle, A., Aertsen, A., & Rotter, S. (2000). Spike count variability in motor cortical neurons. *Eur. J. Neurosci., 12* (suppl. 11), 506.

Newsome, W. T., Britten, K. H., & Movshon, J. A. (1989). Neuronal correlates of a perceptual decision. *Nature, 341*(6237), 52–54.

Nicolelis, M. A. L., Baccala, L. A., Lin, R. C. S., & Chapin, J. K. (1995). Sensorimotor encoding by synchronous neural assembly activity at multiple levels in the somatosensory system. *Science, 268*, 1353–1358.

Palm, G. (1981). Evidence, information and surprise. *Biol. Cybern., 42*, 57–68.

Palm, G. (1990). Cell assemblies as a guidline for brain reseach. *Conc. Neurosci., 1*, 133–148.

Palm, G., Aertsen, A., & Gerstein, G. L. (1988). On the significance of correlations among neuronal spike trains. *Biol. Cybern., 59*, 1–11.

Pauluis, Q. (1999). *Temporal coding in the superior colicullus*. Unpublished doctoral dissertation, Université catholique de Louvain, Brussels, Belgium.

Pauluis, Q., & Baker, S. N. (2000). An accurate measure of the instantaneous discharge probability, with application to unitary joint-event analysis. *Neural Comp., 12*(3), 647–669.

Perkel, D. H., & Bullock, T. H. (1968). Neural coding. *Neurosci. Res. Prog. Bull.*, 6.

Pipa, G., Singer, W., & Grün, S. (2001). Non-parametric significance estimation for unitary events. In N. Elsner & G. M. Kreutzberg (Eds.), *Proc. of the German Neuroscience Society*. Stuttgart: Thieme Verlag.

Press, W. H., Teukolsky, S. A., Vetterling, W. T., & Flannery, B. P. (1992). *Numerical recipes in C* (2nd ed.). Cambridge: Cambridge University Press.

Prut, Y., Vaadia, E., Bergman, H., Haalman, I., Hamutal, S., & Abeles, M. (1998). Spatiotemporal structure of cortical activity: Properties and behavioral relevance. *J. Neurophysiol., 79*(6), 2857–2874.

Riehle, A., Grammont, F., Diesmann, M., & Grün, S. (2000). Dynamical changes and temporal precision of synchronized spiking activity in motor cortex during movement preparation. *J. Physiol. (Paris), 94*(5–6), 569–582.

Riehle, A., Grün, S., Diesmann, M., & Aertsen, A. (1997). Spike synchronization and rate modulation differentially involved in motor cortical function. *Science, 278*, 1950–1953.

Roelfsema, P., Engel, A., König, P., & Singer, W. (1996). The role of neuronal synchronization in response selection: A biologically plausible theory of structured representations in the visual cortex. *J. Cogn. Neurosci., 8*(6), 603–625.

Roy, A., Steinmetz, P., & Niebur, E. (2000). Rate limitations of unitary event analysis. *Neural Comp., 12*, 2063–2082.

Sakurai, Y. (1996). Population coding by cell assemblies—what it really is in the brain. *Neuroscience Research, 26*, 1–16.

Sanes, J. N., & Donoghue, J. P. (1993). Oscillations in local field potentials of the primate motor cortex during voluntary movement. *Proc. Nat. Acad. Sci. USA, 90*, 4470–4474.

Shadlen, M. N., & Newsome, W. T. (1998). The variable discharge of cortical neurons: Implications for connectivity, computation, and information coding. *J. Neurosci., 18*(10), 3870–3896.

Singer, W. (1993). Synchronization of cortical activity and its putative role in information processing and learning. *Annu. Rev. Physiol., 55*, 349–374.

Singer, W. (1999). Neural synchrony: A versatile code for the definition of relations. *Neuron, 24*, 49–65.

Singer, W., Engel, A. K., Kreiter, A. K., Munk, M. H. J., Neuenschwander, S., & Roelfsema, P. R. (1997). Neuronal assemblies: necessity, signature and detectability. *Trends in Cognitive Sciences, 1*(7), 252–261.

Singer, W., & Gray, C. (1995). Visual feature integration and the temporal correlation hypothesis. *Annu. Rev. of Neurosci., 18*, 555–586.

Softky, W. R., & Koch, C. (1993). The highly irregular firing of cortical cells is inconsistent with temporal integration of random EPSPS. *J. Neurosci., 13*, 334–350.

Steinmetz, P., Roy, A., Fitzgerald, P., Hsiao, S., Johnson, K., & Niebur, E. (2000). Attention modulates synchronized neuronal firing in primate somatosensory cortex. *Nature, 404*(6774), 187–190.

Vaadia, E., Haalman, I., Abeles, M., Bergman, H., Prut, Y., Slovin, H., & Aertsen, A. (1995). Dynamics of neuronal interactions in monkey cortex in relation to behavioural events. *Nature, 373*(6514), 515–518.

Villa, A., & Abeles, M. (1990). Evidence for spatiotemporal firing patterns within the auditory thalamus of the cat. *Brain Res., 509*(2), 325–327.

von der Malsburg, C. (1981). *The correlation theory of brain function* (Int. Rep. No. 81-2). Göttingen: Max-Planck-Institute for Biophysical Chemistry.

Received July 20, 2000; accepted April 24, 2001.